© 2022. Published by The Company of Biologists Ltd | Development (2022) 149, dev200045. doi:10.1242/dev.200045

RESEARCH ARTICLE

# RNA-binding FMRP and Staufen sequentially regulate the Coracle scaffold to control synaptic glutamate receptor and bouton development

**Chunzhu Song[1], Shannon N. Leahy[1], Emma M. Rushton[1] and Kendal Broadie[1,2,3,*]**

## ABSTRACT

Both mRNA-binding Fragile X mental retardation protein (FMRP; Fmr1) and mRNA-binding Staufen regulate synaptic bouton formation and glutamate receptor (GluR) levels at the *Drosophila* neuromuscular junction (NMJ) glutamatergic synapse. Here, we tested whether these RNA-binding proteins act jointly in a common mechanism. We found that both *dfmr1* and *staufen* mutants, and trans-heterozygous double mutants, displayed increased synaptic bouton formation and GluRIIA accumulation. With cell-targeted RNA interference, we showed a downstream Staufen role within postsynaptic muscle. With immunoprecipitation, we showed that FMRP binds *staufen* mRNA to stabilize postsynaptic transcripts. Staufen is known to target actin-binding, GluRIIA anchor Coracle, and we confirmed that Staufen binds to *coracle* mRNA. We found that FMRP and Staufen act sequentially to co-regulate postsynaptic Coracle expression, and showed that Coracle, in turn, controls GluRIIA levels and synaptic bouton development. Consistently, we found that *dfmr1*, *staufen* and *coracle* mutants elevate neurotransmission strength. We also identified that FMRP, Staufen and Coracle all suppress pMad activation, providing a *trans*-synaptic signaling linkage between postsynaptic GluRIIA levels and presynaptic bouton development. This work supports an FMRP–Staufen–Coracle–GluRIIA–pMad pathway regulating structural and functional synapse development.

**KEY WORDS: FMRP, Fragile X syndrome, Synaptogenesis, Synapse, Neuromuscular junction, Neurotransmission**

## INTRODUCTION

Fragile X syndrome (FXS) is a common heritable cause of intellectual and autism spectrum disorders (Crawford et al., 2001). FXS patients typically exhibit a fragile X mental retardation 1 (*FMR1*) 5′ untranslated region (UTR) CGG repeat expansion (typically ≥200), which causes epigenetic transcriptional silencing via *FMR1* promoter hypermethylation (Garber et al., 2008; Hansen et al., 1992; Verkerk et al., 1991). The fragile X mental retardation protein (FMRP; FMR1) product is a very broadly expressed (e.g. neurons, muscles) mRNA-binding translation regulator (Drozd et al., 2018), which binds target transcripts via K homology (KH) domains and arginine-glycine rich (RGG) box (Blackwell and Ceman, 2011; Kenny and Ceman, 2016; Myrick et al., 2015; Ramos et al., 2003). FMRP regulates protein translation to modulate synaptic architecture (bouton/spine number) and glutamate receptor (GluR) levels (Comery et al., 1997; Connor et al., 2011). In the *Drosophila* FXS disease model, *dfmr1* mutants likewise exhibit increased synaptic bouton formation and Glutamate receptor IIA (GluRIIA) levels at the neuromuscular junction (NMJ) model glutamatergic synapse (Pan and Broadie, 2007; Zhang et al., 2001). The molecular mechanism of FMRP-mediated synaptic regulation remains elusive; however, FMRP has been increasingly linked to other mRNA-binding proteins (Kenny et al., 2020; Price et al., 2006; Zhang et al., 2017). A key hypothesized partner is Staufen, a double-strand RNA-binding protein (dsRBP) repeatedly associated with FMRP function via both biochemical and genetic interaction studies (Barbee et al., 2006; Chu et al., 2019; Yu et al., 2012).

Staufen plays crucial roles in regulating mRNA localization, stability, translation and ribonucleoprotein (RNP) assembly (Dugré-Brisson et al., 2005; Micklem et al., 2000; Park and Maquat, 2013). In *Drosophila*, Staufen colocalizes with FMRP in neural RNP granules that mediate mRNA translational repression and mRNA decay, with genetic interaction regulating long-term memory consolidation (Barbee et al., 2006; Bolduc et al., 2008). Like FMRP, Staufen controls both synaptic bouton formation and GluRIIA levels at the *Drosophila* NMJ (Gardiol and St Johnston, 2014). In this mechanism, Staufen works by regulating local translation of the 4.1 ezrin-radixin-moesin (FERM) scaffold Coracle in the muscle postsynaptic domain (Gardiol and St Johnston, 2014). Consistently, mammalian Staufen also binds Coracle homolog 4.1 mRNA and is predicted to regulate its local translation (Furic et al., 2008). Coracle is suggested to link F-actin to GluRIIA C-termini to scaffold receptors within the postsynaptic membrane (Chen et al., 2005; McClatchey, 2012). Importantly, intercellular interaction between postsynaptic GluRIIA and the presynaptic bone morphogenic protein (BMP) receptor Wishful thinking (Wit) generates phosphorylated Mothers against decapentaplegic (pMad) retrograde *trans*-synaptic signaling to regulate presynaptic bouton formation (Chou et al., 2020; Sulkowski et al., 2014, 2016). Based on these studies, we hypothesized that FMRP works with Staufen to regulate postsynaptic Coracle scaffolding, which in turn acts to control postsynaptic GluRIIA accumulation and thereby GluRIIA-dependent presynaptic bouton development.

To interrogate this layered hypothesis, we first tested NMJ bouton number and GluRIIA levels in *dfmr1* and *staufen* single mutants and RNA interference (RNAi) lines, to find that both FMRP and Staufen negatively regulate synaptic bouton formation and GluRIIA accumulation. We next made trans-heterozygous double mutants (*dfmr1*/+; *staufen*/+) to find that FMRP and Staufen operate in the same pathway to control synaptic development. Subsequently, we

[1]Department of Biological Sciences, Vanderbilt University and Medical Center, Nashville, TN 37235, USA. [2]Kennedy Center for Research on Human Development, Vanderbilt University and Medical Center, Nashville, TN 37235, USA. [3]Vanderbilt Brain Institute, Vanderbilt University and Medical Center, Nashville, TN 37235, USA.

*Author for correspondence (kendal.broadie@vanderbilt.edu)

C.S., 0000-0003-4459-6929; S.N.L., 0000-0002-2987-6191; K.B., 0000-0003-3783-6023

**Handling Editor: Thomas Lecuit**
**Received 22 July 2021; Accepted 23 March 2022**

Development (2022) 149, dev200045. doi:10.1242/dev.200045

used RNA immunoprecipitation (RIP) to show that FMRP binds *staufen* mRNA to regulate transcript abundance in the postsynaptic muscle, and that Staufen in turn binds *coracle* mRNA. Consistently, Coracle expression in the NMJ postsynaptic domain was elevated in both *dfmr1* and *staufen* mutants, as well as in trans-heterozygous double mutants. We found that postsynaptic Coracle overexpression (OE) and loss of function similarly increase bouton number and GluRIIA levels. Consistently, we employed NMJ electrophysiology recordings to show that *dfmr1*, *staufen* and *coracle* mutants all display increased synaptic strength. Moreover, postsynaptic knockdown of *dfmr1*, *staufen* and *coracle* all caused elevated presynaptic pMad levels, consistent with activation of GluRIIA–Wit retrograde *trans*-synaptic signaling to drive presynaptic bouton formation. Taken together, these findings suggest that FMRP and Staufen work sequentially to inhibit the Coracle scaffold controlling GluRIIA levels in postsynaptic domain, and that postsynaptic GluRIIA levels in turn signal presynaptic bouton development. This work provides insights into the molecular pathway by which FMRP regulates synapse formation, identifying potential new FXS treatment targets.

## RESULTS

### FMRP and Staufen negatively regulate synaptic bouton formation and GluRIIA levels

At the *Drosophila* NMJ, we have previously reported that viable *dfmr1* nulls ($dfmr1^{50M}$) exhibit elevated synaptic bouton formation and GluRIIA levels (Pan and Broadie, 2007; Zhang et al., 2001). By contrast, *staufen* nulls are embryonic lethal owing to essential mRNA localization and translation roles (St Johnston et al., 1991), and a viable *staufen* mutant over a genomic deficiency [$stau^{HL}$/*Df(2R)Pcl7B*] reportedly develops fewer NMJ boutons and lower GluRIIA levels (Gardiol and St Johnston, 2014). The $stau^{HL}$ mutant contains a T-A point mutation in dsRNA-binding domain 5 (Fig. S1A) that blocks local translation (Gardiol and St Johnston, 2014). As a first step, we re-tested $dfmr1^{50M}$ and $stau^{HL}$ mutants compared with matched genetic background controls ($w^{1118}$) for bouton number and GluRIIA level. We then tested trans-heterozygotes ($dfmr1^{50M}$/+; $stau^{HL}$/+) for a predicted interaction within the same pathway. We assayed wandering third-instar NMJs double labeled with anti-horseradish peroxidase (HRP) (Jan and Jan, 1982; Pan and Broadie, 2007), which recognizes neural presynaptic membrane, and anti-Discs large (DLG; Dlg1) (Kamimura et al., 2019; Menon et al., 2013), which recognizes muscle subsynaptic reticulum (SSR). Both total NMJ boutons and developing satellite boutons were counted in muscle 4 terminals in abdominal segment A3. The same genotypes were double labeled with anti-HRP and anti-GluRIIA (Pan and Broadie, 2007) at the same NMJ. GluRIIA labeling intensity was quantified at HRP-thresholded boutons.

Compared with the genetic background control ($w^{1118}$), $dfmr1^{50M}$ mutants showed supernumerary synaptic bouton formation (Fig. 1A, top). The quantified total bouton number was significantly elevated (mean±s.e.m.: control 19.10±1.77, *dfmr1* 31.42±1.67; $P<0.0001$; Fig. 1C), with a parallel increase in satellite boutons (number/NMJ: control 0.86±0.27, *dfmr1* 2.65±0.47; $P=0.003$; Fig. 1D). Similarly, $stau^{HL}$ mutants also developed consistently more NMJ boutons compared with $w^{1118}$ genetic controls (Fig. 1A, bottom). Quantification showed that the total NMJ bouton number was significantly increased in *staufen* mutants compared with controls (control 20.85±0.78, $stau^{HL}$ 29.25±2.15; $P=0.0003$; Fig. 1C), with satellite boutons also elevated (control 0.89±0.21, $stau^{HL}$ 4.64±0.72; $P<0.0001$; Fig. 1D). Assaying synaptic GluRIIA levels, *dfmr1* mutants exhibited a clear increase throughout the NMJ terminal (Fig. 1B, top). GluRIIA fluorescence levels normalized to control were significantly higher in *dfmr1* mutants (control 1.00±0.08, $dfmr1^{50M}$ 1.616±0.11; $P=0.0002$; Fig. 1E). Likewise, GluRIIA levels were also increased in the *staufen* mutants compared with matched controls (Fig. 1B). Compared with levels in genetic controls, the normalized GluRIIA fluorescence levels in the *staufen* mutants were also significantly elevated (control 1.00±0.04, $stau^{HL}$ 1.24±0.06; $P=0.0014$; Fig. 1B,E). These results indicate that FMRP and Staufen similarly regulate synaptic development.

To further test *staufen* phenotypes, we next used *staufen* RNAi as an independent knockdown method (Table S1, Fig. S1B-D). Studies with quantitative PCR (qPCR) showed ∼90% *staufen* mRNA loss with global UH1-Gal4 driving UAS-*staufen* RNAi [Vienna *Drosophila* Resource Center (VDRC) 106645; Fig. S1B]. Consistent with the above *staufen* mutants, *staufen* RNAi elevated both presynaptic bouton formation (Fig. S2A, top) and postsynaptic GluRIIA levels (Fig. S2A, bottom). Quantification of the knockdown showed that UH1>*stau* RNAi (VDRC 106645) increased all measurements, including total bouton number (UH1/+ 23.33±1.09, UH1>*stau* RNAi 28.87±1.30; $P=0.004$; Fig. S2B), satellite boutons (UH1/+ 1.33±0.43, UH1>*stau* RNAi 2.93±0.50; $P=0.0273$; Fig. S2C) and GluRIIA levels (UH1/+ 1.00±0.06, UH1>*stau* RNAi 1.28±0.07; $P=0.0038$; Fig. S2D). We repeated these analyses with an independent *staufen* RNAi line [Bloomington *Drosophila* Stock Center (BDSC) 31247]. Consistent with the above results, this second RNAi similarly caused a significant increase in synaptic bouton number (UH1/+ 24.33±0.79, UH1>*stau* RNAi 32.36±1.815, $P=0.0004$) and GluRIIA levels (UH1/+ 1.00±0.07, UH1>*stau* RNAi 1.66±0.16; $P=0.0041$). Thus, $stau^{HL}$ and two independent *staufen* RNAi lines (VDRC 106645 and BDSC 31247) confirmed the same NMJ development phenotypes. We therefore conclude that Staufen loss increases synaptic bouton formation and GluRIIA levels, consistent with FMRP requirements.

To test the hypothesis that FMRP and Staufen co-regulate NMJ development in a common pathway, we next made *dfmr1* and *staufen* double mutants. Homozygous double mutants were early larval lethal, but $dfmr1^{50M}$/+; $stau^{HL}$/+ trans-heterozygotes were viable and could be tested. Similar to $dfmr1^{50M}$ and $stau^{HL}$ single mutants, we found a clear elevation of total boutons in the trans-heterozygotes. Quantification showed bouton increases in *dfmr1* (control 17.91±0.89, *dfmr1*/+ 25.88±1.81) and *staufen* (control 19.00±0.70, *stau*/+ 26.91±1.56) heterozygotes, and the trans-heterozygotes (control 17.56±1.17, *dfmr1*/+; *stau*/+ 28.70±1.55; $P<0.0001$; Fig. 2A, bottom). We next tested GluRIIA to find similar levels in *dfmr1*/+ and *stau*/+ heterozygotes compared with controls, but elevated levels in *dfmr1*/+; *stau*/+ trans-heterozygotes (Fig. 2A). Quantified GluRIIA levels were not changed in either *dfmr1*/+ or *stau*/+ single heterozygotes compared with control (Fig. 2A,B), but were significantly increased in trans-heterozygotes (normalized control 1.00±0.08, *dfmr1*/+; *stau*/+ 1.28±0.12; $P=0.047$; Fig. 2A,B). These findings showed that reducing FMRP and Staufen in parallel elevated synaptic GluRIIA levels, suggesting that the two RNA-binding proteins (RBPs) work in a common mechanism. Overall, we conclude that FMRP and Staufen negatively regulate synaptic development in the same direction, and to a similar degree, by functioning in the same pathway.

### Postsynaptic Staufen regulates GluRIIA levels and presynaptic bouton development

Cell-targeted RNAi studies have established that FMRP inhibits GluRIIA levels only postsynaptically (Pan and Broadie, 2007),

Development (2022) 149, dev200045. doi:10.1242/dev.200045

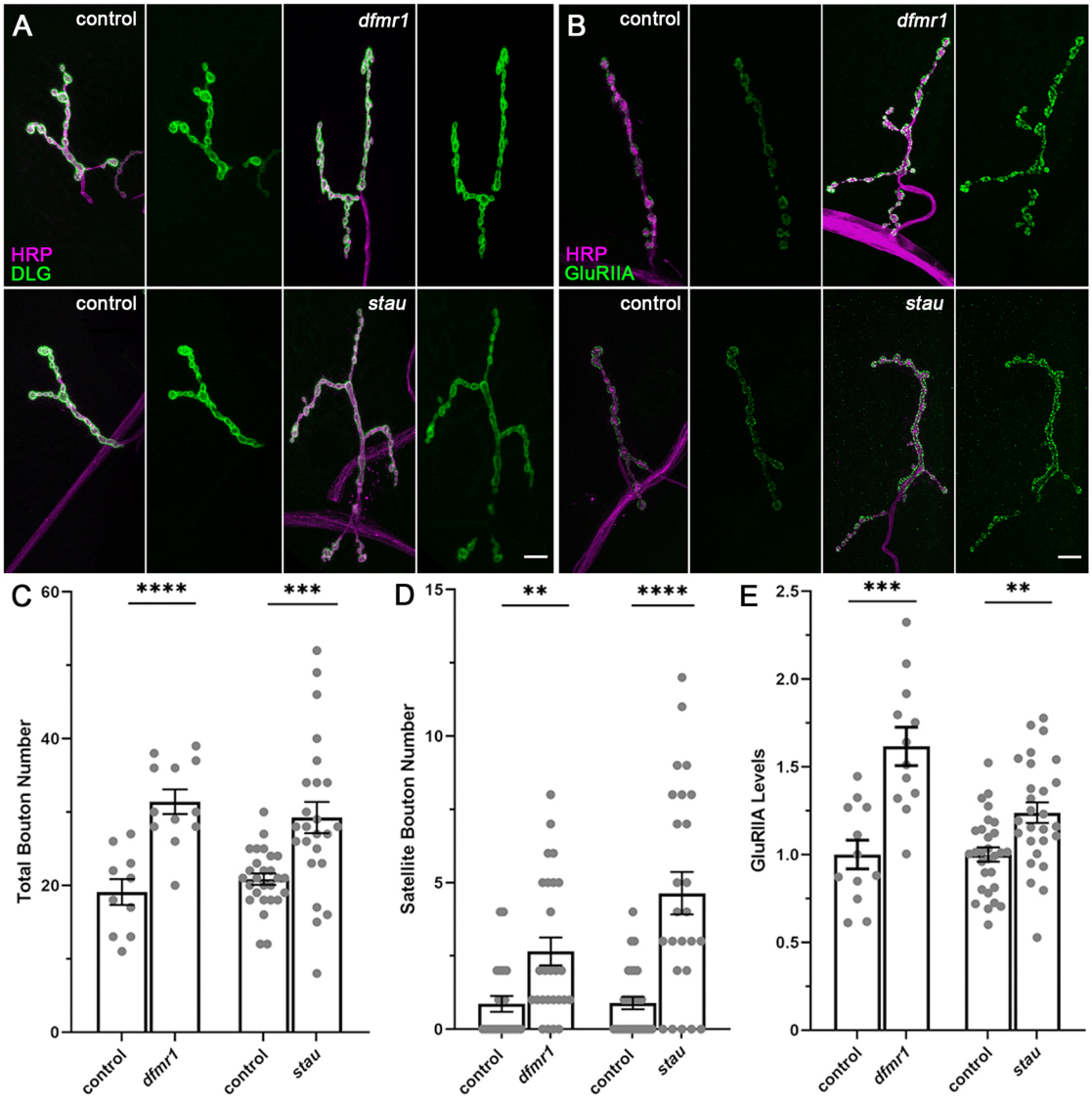


**Fig. 1. FMRP and Staufen both limit neuromuscular junction (NMJ) bouton formation and GluRIIA levels.** Larval NMJ synaptic terminals compared between genetic background control ($w^{1118}$), *dfmr1* ($dfmr1^{50M}$) and *staufen* ($stau^{HL}$) mutants. (A) Double labeling for the presynaptic anti-horseradish peroxidase (HRP; magenta) and the postsynaptic anti-Discs large (DLG; green), with overlap shown in white. (B) Double labeling for HRP (magenta) and anti-Glutamate receptor IIA (GluRIIA; green), with overlap shown in white. (C) Quantification of total synaptic bouton number in muscle 4 type 1 NMJ terminals, with each mutant and control paired for side-by-side comparisons. (D) Quantification of satellite bouton number only within each type 1 synaptic terminal. (E) Quantification of GluRIIA fluorescence intensity normalized to genetic background control. In all figures, graphs show dot plots of all individual data points and histogram bars of the mean±s.e.m., with statistical comparisons using unpaired two-tailed Student's *t*-tests. ***P*<0.01, ****P*<0.001 and *****P*<0.0001. Scale bars: 10 µm.

but suppresses bouton development in both postsynaptic and presynaptic cells (Friedman et al., 2013; Zhang et al., 2001). Likewise, Staufen subcellularly localizes in the postsynaptic domain, to function postsynaptically in muscle, controlling mRNA localization and local translation (Gardiol and St Johnston, 2014). These previous studies, as well as the above non-complementation genetic interaction tests, suggest that FMRP interacts with Staufen in the postsynaptic compartment to regulate GluRIIA levels and presynaptic bouton formation. Previous antibody labeling shows Staufen in the postsynaptic muscle region immediately surrounding NMJ termini, with Staufen not detectable in presynaptic boutons (Gardiol and St Johnston, 2014). We therefore hypothesized Staufen that has a specific muscle postsynaptic function. To test this hypothesis, we used muscle-specific 24B-Gal4 (Kim et al., 2021) and neuron-specific *elav*-Gal4 (Kan et al., 2021) to drive UAS-*staufen* RNAi (VDRC 106645; Landskron et al., 2018). We also used postsynaptic 24B-Gal4 to drive wild-type UAS-*staufen* in both homozygous $stau^{HL}$ and $dfmr1^{50M}$ mutants. As above, synaptic bouton development was tested with presynaptic anti-HRP and postsynaptic anti-DLG double labeling, and GluRIIA levels with anti-HRP and anti-GluRIIA double labeling.

Compared with transgenic controls (24B-Gal4/+), muscle-targeted *staufen* RNAi (24B>*stau* RNAi) resulted in more synaptic boutons (Fig. 3A, top). With quantification, total boutons were significantly increased in 24B>*stau* RNAi (24B/+ 21.94±1.23, RNAi 25.43±0.86; *P*=0.02; Fig. 3C), with more developing satellite boutons (24B/+ 2.09±0.31, RNAi 3.46±0.34; *P*=0.0047; Fig. 3D). By contrast, neural *staufen* knockdown (*elav*>*stau* RNAi) had no effect, with no change in bouton number (Fig. 3A, bottom). Quantification showed no significant difference in synaptic bouton formation between transgenic control (*elav*-Gal4/+) and neural

Development (2022) 149, dev200045. doi:10.1242/dev.200045

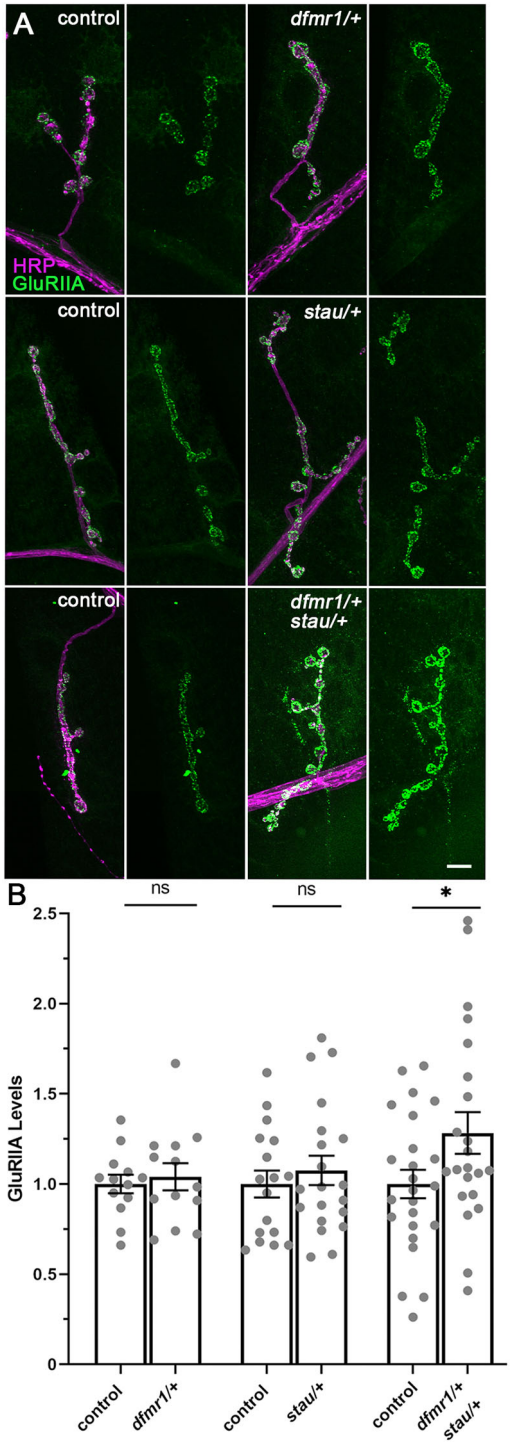


**Fig. 2. FMRP and Staufen work together to co-regulate synaptic GluRIIA levels.** Larval NMJ synaptic terminals in controls ($w^{1118}$) compared with the single heterozygous *dfmr1* ($dfmr1^{50M}$/+) and *staufen* ($stau^{HL}$/+) mutants, and the double trans-heterozygous combination ($dfmr1^{50M}$/+; $stau^{HL}$/+). (A) Double labeling for presynaptic HRP (magenta) and GluRIIA (green) with each mutant condition paired to genetic background control. Scale bar: 10 µm.
(B) Quantification of GluRIIA fluorescence intensity normalized to control. ns, not significant (for both single heterozygous conditions); *$P$<0.05 (for the double trans-heterozygous mutant).

*staufen* RNAi ($P$=0.91; Fig. 3C), indicating that presynaptic Staufen has no detectable role. Assaying GluRIIA levels, muscle-targeted knockdown (24B>*stau* RNAi) resulted in clearly higher fluorescence than in the transgenic controls (24B-Gal4/+), with elevated GluRIIA levels at synaptic boutons (Fig. 3B, top). Quantified GluRIIA measurements showed that muscle-targeted *staufen* RNAi strongly upregulated GluIIA levels compared with normalized controls (24B/+ 1.00±0.04, RNAi 1.33±0.05; $P$<0.0001; Fig. 3E). By contrast, neural *staufen* knockdown (*elav*>*stau* RNAi) resulted in no detectable change in GluRIIA synaptic fluorescence (Fig. 3B, bottom), with quantified results showing no role in determining GluRIIA levels ($P$=0.46; Fig. 3E). These findings suggest that Staufen acts in the postsynaptic muscle to regulate NMJ development.

To further test this conclusion, we next performed complementary *staufen* rescue experiments in the postsynaptic muscle. Compared with transgenic control (24B-Gal4/+), muscle UAS-*staufen* expression in $stau^{HL}$ ($stau^{HL}$) homozygous mutant ($stau^{HL}$; 24B>*stau*) showed strongly rescued synaptic development (Fig. S3). With targeted postsynaptic UAS-*staufen*, the presynaptic bouton number was restored to the control level (24B/+ 23.80±0.86, $stau^{HL}$; 24B>*stau* 26.89±1.24), with no significant difference remaining ($P$=0.113). Assaying GluRIIA levels revealed an even stronger effect, with muscle-targeted rescue ($stau^{HL}$; 24B>*stau*) resulting in clearly reduced fluorescence compared with that of transgenic controls (24B-Gal4/+), showing lower GluRIIA levels at synaptic boutons (Fig. S3A). Quantification revealed a >40% reduction in GluRIIA receptors normalized to transgenic controls (24B/+ 1.00±0.067, $stau^{HL}$; 24B>*stau* 0.57±0.04), which is a significant decrease ($P$<0.0001; Fig. S3B). Consistent with this postsynaptic requirement, the same muscle *staufen* OE in the null *dfmr1* homozygous mutant (*dfmr1*; 24B>*stau*) suppressed GluRIIA expression to levels comparable with those of the transgenic control (normalized 24B/+ 1.00±0.07, *dfmr1*; 24B>*stau* 1.21±0.19; $P$=0.21). Taken together, these findings suggest that FMRP interacts with Staufen in the muscle postsynaptic domain to regulate GluRIIA levels.

### FMRP binds *staufen* mRNA and downstream Staufen protein binds *coracle* mRNA

FMRP and Staufen both bind mRNA directly to regulate local protein translation (Bonnet-Magnaval, 2016; Laver et al., 2013; Liu et al., 2018; Tsang et al., 2019), and therefore could operate either in parallel or sequentially in protein-mRNA interactions limiting synaptic development. Importantly, FMRP has been predicted to bind *staufen* mRNA (D'Annessa et al., 2019), and we therefore hypothesized that FMRP regulates Staufen translation in a sequential mechanism. To test the predicted FMRP and *staufen* mRNA interaction, we used UH1-Gal4 to express UAS-*dfmr1*::YFP (Cziko et al., 2009), and then pulled down FMRP-RNA complexes from larval lysates using anti-YFP beads (Nagai et al., 2002; Rana et al., 2018). In parallel, non-tagged $w^{1118}$ third-instar lysates served as the immunoprecipitation (IP) negative control. In both cases, α-Tubulin (αTub85E; FMRP does not bind) was the negative control and Futsch (a known FMRP target) was the positive control (Zhang et al., 2001). Immunoprecipitated mRNAs were reverse transcribed using random hexamers, followed by specific primer PCR amplification to produce ∼200 bp PCR fragments (Table S2). Downstream of hypothesized mRNA binding, we also assayed *staufen* mRNA levels with qPCR measurements in *dfmr1* null mutants and with muscle-targeted *dfmr1* RNAi (Flockhart et al., 2006) to test the postsynaptic interaction in isolated muscle analyses.

The FMRP IP pulled down *staufen* mRNA from larval lysates (Fig. 4A, IP, top). Consistently, the *futsch* mRNA positive control was precipitated in parallel, with no detectable binding to the *α*-

Development (2022) 149, dev200045. doi:10.1242/dev.200045

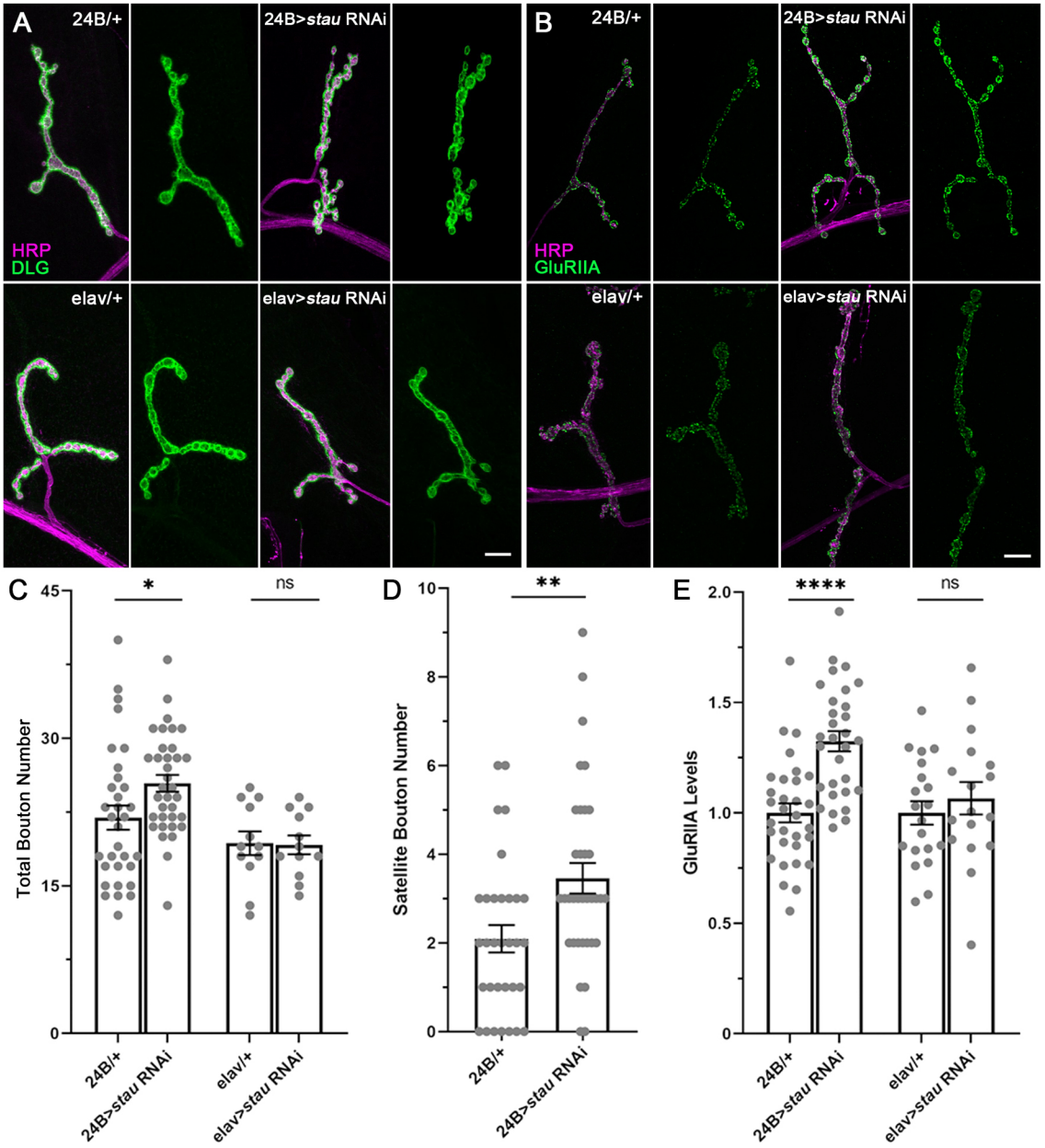


**Fig. 3. Postsynaptic Staufen regulates NMJ bouton formation and GluRIIA levels.** Larval NMJ synaptic terminals in transgenic controls compared with postsynaptic muscle Staufen RNAi (24B>*stau* RNAi) and presynaptic neuron Staufen RNAi (*elav>stau* RNAi). (A) Double labeling for HRP (magenta) and DLG (green), with the 24B-Gal4 control (left) and RNAi (right) shown in the top row and the *elav*-Gal4 control/RNAi in the bottom row. (B) Double labeling for HRP (magenta) and GluRIIA (green) for the same comparisons. (C,D) Quantification of total NMJ bouton number (C) and satellite bouton number (D) on muscle 4 for all four conditions. (E) Quantification of GluRIIA fluorescent intensity normalized to the transgenic controls. **P*<0.05, ***P*<0.01 and *****P*<0.0001; ns, not significant (for *elav>stau* RNAi). Scale bars: 10 µm.

*tubulin* mRNA negative control (Fig. 4A). As expected, the genetic negative control $w^{1118}$ (no YFP) showed no immunoprecipitated bands (Fig. 4A, IP, bottom). These results indicated that FMRP binds to *staufen* mRNA from the wandering third instar, with the controls confirming the binding interaction specificity. RNA binding protects transcripts from degradation by increasing RNA stability, so we hypothesized that FMRP binding should increase *staufen* mRNA levels. To test this idea, we performed qPCR to measure *staufen* mRNA levels in genetic background controls ($w^{1118}$) compared with *dfmr1* nulls (Fig. 4B). Quantification showed that *staufen* mRNA levels were significantly reduced in *dfmr1* mutants normalized to controls (control 1.00±0.05, *dfmr1* 0.68±0.08; *P*=0.002; Fig. 4B). This finding suggested that FMRP stabilizes *staufen* mRNA through protein-RNA binding. To test postsynaptic roles, we used muscle 24B-Gal4 to drive *dfmr1* RNAi, and then isolated body muscles for mRNA extraction (Fig. 4C). Quantified qPCR results showed that *staufen* mRNA levels were strongly downregulated in 24B>*dfmr1* RNAi muscles normalized to the transgenic control (24B/+ 1.00±0.09, RNAi 0.61±0.10; *P*=0.009; Fig. 4C). These findings suggest that FMRP binding stabilizes *staufen* mRNA in the postsynaptic muscle.

At the NMJ, postsynaptic Staufen is required for the localization and translation of *coracle* mRNA, which encodes a mammalian 4.1 ortholog functioning as a GluRIIA anchoring scaffold (Gardiol and

Development (2022) 149, dev200045. doi:10.1242/dev.200045

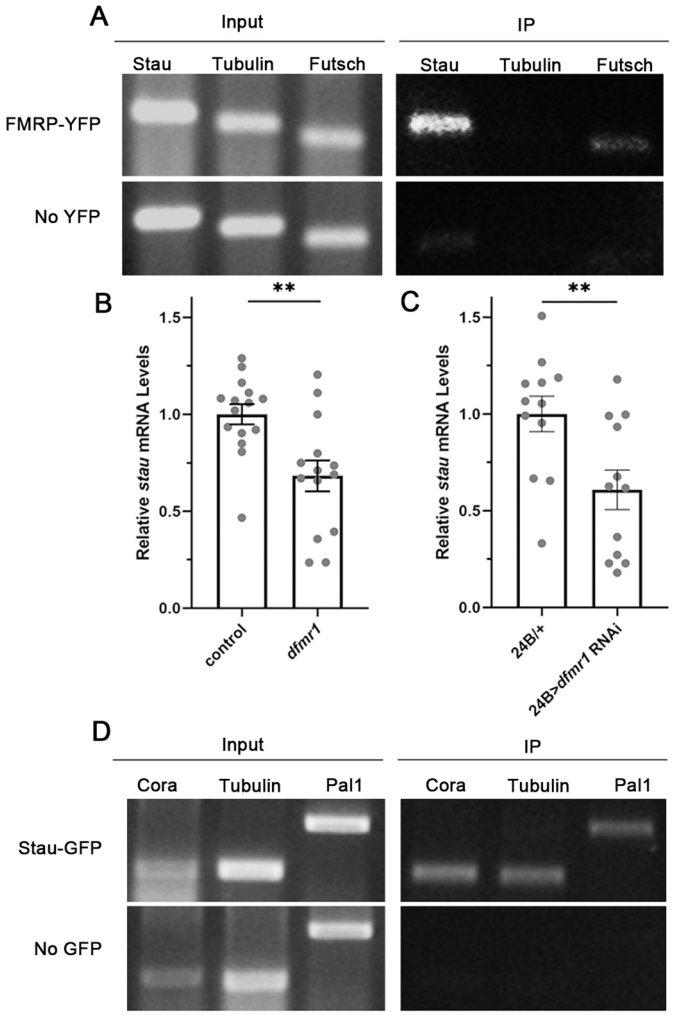


**Fig. 4. FMRP binds/stabilizes *staufen* mRNA and Staufen binds *coracle* mRNA.** Larval musculature RNA immunoprecipitation (RIP) assays for FMRP and Staufen show transcript binding interactions. (A) FMRP-YFP immunoprecipitated by anti-YFP (top) compared with $w^{1118}$ negative control (no YFP, bottom). The input is shown on the left and the immunoprecipitate (IP) on the right, for Staufen, α-Tubulin (negative control) and Futsch (positive control). (B) qPCR measurements of *stau* mRNA levels in *dfmr1* mutant larvae normalized to genetic background control ($w^{1118}$). (C) Muscle *stau* mRNA levels with muscle-targeted *dfmr1* RNAi (24B>*dfmr1* RNAi) normalized to transgenic control (24B-Gal4/+). (D) Staufen-GFP immunoprecipitated by anti-GFP (top) compared with $w^{1118}$ negative control (no GFP, bottom). The input (left) and IP (right) are shown for Coracle, α-Tubulin and Pal1. $^{**}P<0.01$.

St Johnston, 2014). To test Staufen and *coracle* mRNA interaction, we used UH1-Gal4 to drive UAS-*staufen*::GFP (Barbee et al., 2006; Laver et al., 2013) and pulled down RNA complexes from larval lysates using anti-GFP beads (Fig. 4D). As above, $w^{1118}$ (no GFP) was the IP negative control. As a positive control, Staufen binds *α-tubulin* mRNA (Laver et al., 2013), whereas *peptidyl-α-hydroxyglycine-α-amidating lyase 1* (*Pal1*) mRNA reportedly is not bound by Staufen (Laver et al., 2013) and was therefore selected as a negative control. Staufen IP pulled down *coracle* mRNA, but also pulled down *α-tubulin* and *Pal1* mRNA (Fig. 4D). We also tested *GAPDH* (*Gapdh2*), *RP49* (*RpL32*) and *Gal4* mRNAs, and all of these were also immunoprecipitated. Repeated trials with increasing transfer RNA (tRNA) concentrations (300 µg, 600 µg, 900 µg, 1 mg) or even highly elevated tRNA (10 mg, 20 mg) all showed continued mRNA pulldown. Thus, Staufen binds *coracle* mRNA, but lacks binding specificity. Staufen is also predicted to bind *dfmr1* mRNA (Laver et al., 2013), but FMRP levels did not change in *staufen* mutant muscle (control 1.00±0.04, $stau^{HL}$ 0.91±0.07; $P$=0.30; Fig. S4A,B). We therefore suggest that there is a directional pathway of FMRP binding *staufen* mRNA to control postsynaptic muscle levels, with Staufen in turn binding *coracle* mRNA.

### FMRP and Staufen act sequentially to regulate postsynaptic Coracle expression

The Staufen dsRNA-binding domain 5 is specifically required for Coracle local translation (Gardiol and St Johnston, 2014). Disruption of this domain in $stau^{HL}$ over the genomic deficiency [$stau^{HL}$/*Df(2R)Pcl7B*] reportedly impairs postsynaptic accumulation of Coracle protein via loss of local translation, without affecting *coracle* mRNA localization (Gardiol and St Johnston, 2014), suggesting that Staufen regulates local Coracle translation specifically within the NMJ postsynaptic domain. Coracle binds the GluRIIA C-terminus to scaffold receptors in the postsynaptic membrane, with tight stoichiometry between Coracle and GluRIIA levels within muscle (Chen et al., 2005). As FMRP and Staufen both repress GluRIIA accumulation, we hypothesized that both proteins should inhibit postsynaptic Coracle expression. To test how FMRP and Staufen might regulate Coracle, alone and in combination within the FMRP-Staufen pathway, we used an anti-Coracle antibody (Gomez et al., 2012) to measure levels in anti-HRP-labeled NMJs in wandering third instars. Coracle levels were measured in genetic background controls ($w^{1118}$), *dfmr1* and *staufen* homozygous mutants, *dfmr1*/+ and *staufen*/+ heterozygotes, and *dfmr1*/+; *stau*/+ trans-heterozygous double mutants. The expression was quantified postsynaptically surrounding anti-HRP thresholded synaptic boutons, within a dilated 1 µm region of interest to capture the postsynaptic SSR domain.

Coracle encircled NMJ boutons, with a more intense ring in *dfmr1* mutants than in controls (Fig. 5A). Quantification showed that normalized Coracle levels were significantly elevated in *dfmr1* mutants (control 1.00±0.18, *dfmr1* 1.68±0.13; $P$=0.0081; Fig. 5B). To test possible feedback regulation, we assayed anti-FMRP in *coracle* mutant muscle, but found no detectable change (control 1.00±0.10, *cora* 1.14±0.12; $P$=0.36; Fig. S4C,D), showing that FMRP acts upstream of Coracle. Compared with genetic controls ($w^{1118}$), *stau* mutants also had more intense Coracle rings around boutons (Fig. 5C). Quantification showed that *staufen* mutants also exhibited significantly more postsynaptic Coracle expression (control 1.00±0.08, *stau* 1.32±0.05; $P$=0.0018; Fig. 5D). These findings indicate that FMRP and Staufen similarly limit Coracle in the NMJ postsynaptic domain. To test FMRP and Staufen action in the same pathway, we assayed *dfmr1*/+; *stau*/+ trans-heterozygotes. Neither *dfmr1*/+ nor *stau*/+ single heterozygotes showed any detectable difference in Coracle levels compared with controls (Fig. S5A-D). By contrast, the *dfmr1*/+; *stau*/+ trans-heterozygotes had clearly enhanced postsynaptic Coracle rings around NMJ boutons (Fig. 5E). Quantification showed that the double mutant had a significant 50% increase in normalized Coracle levels compared with the control (control 1.00±0.14, *dfmr1*/+; *stau*/+ 1.53±0.20; $P$=0.034; Fig. 5F). We suggest that FMRP and Staufen act sequentially to inhibit Coracle GluRIIA-scaffold enrichment in the postsynaptic domain.

### Postsynaptic Coracle regulates GluRIIA levels and presynaptic bouton formation

Null *coracle* mutants are embryonic lethal (Lamb et al., 1998), and total Coracle loss impairs GluRIIA accumulation at the embryonic

Development (2022) 149, dev200045. doi:10.1242/dev.200045

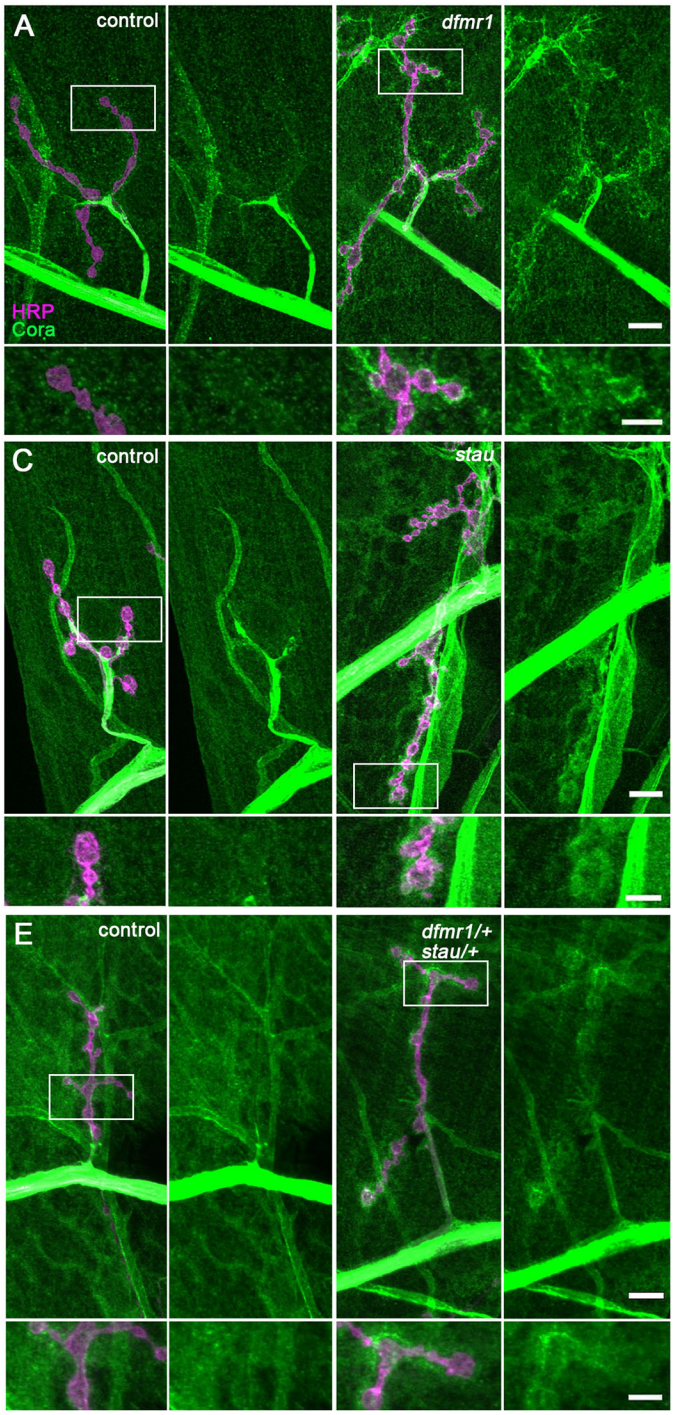


**Fig. 5. FMRP and Staufen act to co-regulate postsynaptic Coracle expression.** Larval NMJ synaptic terminals labeled for Coracle in controls ($w^{1118}$), *dfmr1* ($dfmr1^{50M}$) and *staufen* ($stau^{HL}$) mutants, and double trans-heterozygotes ($dfmr1^{50M}$/+; $stau^{HL}$/+). Top rows show full muscle 4 NMJs (scale bars: 10 µm) and white-boxed regions are shown magnified below (scale bars: 5 µm). (A) Double labeling for presynaptic HRP (magenta) and Coracle (Cora; green) in control versus *dfmr1* mutant. (B) Postsynaptic Coracle levels are normalized to control. (C) Coracle labeling shown in a *staufen* mutant. (D) Postsynaptic Coracle levels normalized to control. (E) Coracle labeling shown in the double trans-heterozygote ($dfmr1^{50M}$/+; $stau^{HL}$/+). (F) Postsynaptic Coracle levels shown normalized to control. *$P$<0.05 and **$P$<0.01. The single heterozygotes ($dfmr1^{50M}$/+ and $stau^{HL}$/+) are shown in Fig. S4.

NMJ (Chen et al., 2005). As a GluRIIA-binding scaffold, Coracle anchors receptors to underlying F-actin cytoskeleton in the postsynaptic domain (Chen et al., 2005). Consistently, our above results predicted that Coracle OE should be causally associated with an increase in postsynaptic GluRIIA levels. However, many scaffolds like Coracle show similar phenotypes with loss and OE (McCarthy, 2010), including scaffolds at intercellular junctions (Tokuda et al., 2014) and specifically at neuronal synapses (Fulterer et al., 2018). We therefore hypothesized that disrupting Coracle levels in either direction could generate elevated GluRIIA levels and, secondarily, supernumerary bouton formation. To test this hypothesis, we assayed in parallel a larval viable *coracle* hypomorphic mutant ($cora^{14}$; Khadilkar et al., 2017; Lamb et al., 1998) and muscle-targeted 24B-Gal4 *coracle* RNAi (Jiang et al., 2019), as well as *coracle* OE (Ward et al., 1998). For all three conditions and matched controls, we used double labeling with presynaptic anti-HRP and postsynaptic anti-DLG to assay NMJ architecture and quantify synaptic bouton number. We also double labeled with anti-HRP and anti-GluRIIA to assay synaptic GluRIIA expression and quantify receptor level based on fluorescence intensity.

Both *coracle* mutants and muscle-targeted *coracle* RNAi produced enlarged NMJs with more synaptic boutons (Fig. 6A). Quantification showed that bouton numbers increase in *coracle*

Development (2022) 149, dev200045. doi:10.1242/dev.200045

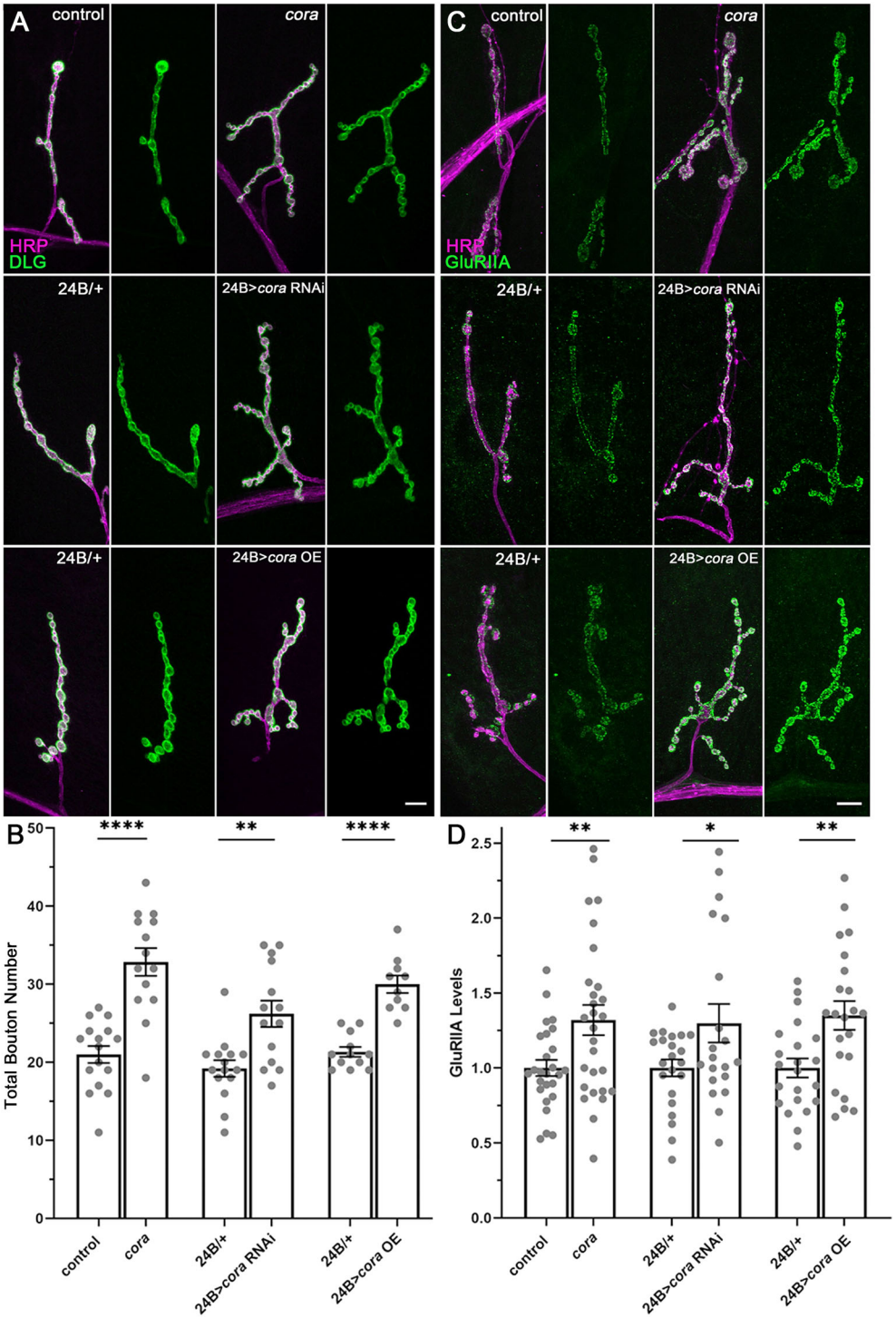


**Fig. 6. Postsynaptic Coracle regulates NMJ bouton growth and GluRIIA levels.** Larval NMJ synaptic terminal structure and GluRIIA levels compared between genetic background controls ($w^{1118}$), *coracle* (*cora*$^{14}$) mutants, postsynaptic *coracle* knockdown (24B>*cora* RNAi) and postsynaptic *coracle* overexpression (24B>*cora* OE). (A) Double labeling for presynaptic HRP (magenta) and postsynaptic DLG (green) in all genotypes. (B) Quantification of synaptic bouton number at the muscle 4 NMJ. (C) Double labeling for HRP (magenta) and GluRIIA (green) in all the above genotypes. (D) Quantification of GluRIIA fluorescence intensity normalized to controls. **P*<0.05, ***P*<0.01 and *****P*<0.0001. Scale bars: 10 µm.

mutants (control 21.00±1.10, *cora*$^{14}$ 32.86±1.79; *P*<0.0001) and with muscle *coracle* RNAi (24B/+ control 19.20±1.06, RNAi 26.21±1.69; *P*=0.0014; Fig. 6B). NMJ bouton formation was also elevated by muscle-specific *coracle* OE (Fig. 6A, bottom). Quantification showed that bouton number was significantly elevated by 24B-Gal4-targeted *coracle* OE (24B/+ 21.33±0.64, *cora* OE 30.00±1.12; *P*<0.0001; Fig. 6B). Thus, both Coracle loss and gain in the postsynaptic muscle similarly restricts presynaptic development. Similarly, *coracle* mutants, muscle-targeted *coracle* RNAi and OE all had more postsynaptic GluRIIA than controls (Fig. 6C). Quantification showed that normalized GluRIIA levels were significantly higher in *coracle* mutants (control 1.00±0.05, *cora*$^{14}$ 1.32±0.10; *P*=0.0085) and muscle-specific 24B-Gal4>*cora* RNAi (24B/+ 1.00±0.06, RNAi 1.30±0.13; *P*=0.03; Fig. 6D) than in controls. Supporting our hypothesis, quantification likewise showed that normalized GluRIIA levels were highly elevated by *coracle* OE in muscle (24B/+ 1.00±0.06, *cora* OE 1.35±0.096; *P*=0.004; Fig. 6D). Taken together, these results suggest that postsynaptic FMRP restricts Staufen to restrict Coracle to restrict GluRIIA levels and thus presynaptic bouton formation, with loss and gain of Coracle phenocopying each other within this GluRIIA regulative mechanism.

Development (2022) 149, dev200045. doi:10.1242/dev.200045

### FMRP, Staufen and Coracle all negatively regulate synaptic functional differentiation

Clustered postsynaptic GluRIIA channels mediate excitatory ion influx during neurotransmission (Han et al., 2015; Müller and Davis, 2012). GluRIIA levels are thus positively correlated with enhanced excitatory synaptic strength (Petzoldt et al., 2014). We therefore hypothesized that impairment of the FMRP–Staufen–Coracle pathway should elevate function. To test this hypothesis, two-electrode voltage-clamp (TEVC) recordings in *dfmr1*, *staufen* and *coracle* mutants were compared with those in genetic background controls ($w^{1118}$). Evoked excitatory junction current (EJC) amplitude provides a measure of overall NMJ neurotransmission efficacy dependent on postsynaptic GluRs precisely juxtaposed to the presynaptic active zone glutamate release sites (Clarke et al., 2012; Hong et al., 2020; Marrus, 2004). To make EJC recordings, suprathreshold stimuli (0.5 ms) were applied with a motor nerve suction electrode at 0.2 Hz (Kopke et al., 2020). Ten sequential evoked traces were recorded in 1 mM [$Ca^{2+}$] and averaged to generate each data point (Kopke et al., 2020). Miniature EJC (mEJC) recordings assay spontaneous synaptic vesicle fusion events, with frequency indicating presynaptic fusion probability and amplitude correlated with postsynaptic GluR function (Harris and Littleton, 2015). In these recordings, mEJCs were analyzed at 10 kHz in continuous gap-free configuration (Kopke et al., 2020).

Compared with the EJC amplitude of the genetic control ($w^{1118}$), *dfmr1*, *staufen* and *coracle* mutants all showed consistently elevated EJC amplitudes (Fig. 7A). Relative to the control EJC amplitude (126.9±11.75 nA), NMJ synaptic strength was significantly greater in *dfmr1* (190.0±19.19; $P$=0.0069), *staufen* (185.0±11.24; $P$=0.0091) and *coracle* (206.7±12.59; $P$=0.0002) mutants (Fig. 7B), consistent with their GluRIIA accumulation. Spontaneous mEJC events failed to reveal any obvious changes in these mutants (Fig. 7C). The mEJC frequency was not detectably altered, and quantification showed no change in mutants (*staufen*: $P$=0.92; *coracle*: $P$=0.67; Fig. 7D), indicating that synapse number and presynaptic vesicle fusion probability were unaltered. The mEJC amplitude was also unchanged in mutants (Fig. 7C), and quantification showed no change in mutants (*staufen*: $P$=0.41; *coracle*: $P$=0.93; Fig. 7E), indicating that GluR conductance was unaffected. Similar EJC-specific phenotypes have been repeatedly reported at the *Drosophila* NMJ (e.g. Wang et al., 2017), which might reflect postulated differences between evoked and spontaneous fusion mechanisms (Horvath et al., 2020; Kavalali, 2015) or compensatory interactions between GluRIIA number and conductance (Petzoldt et al., 2014; Renden and Broadie, 2003). We conclude that FMRP, Staufen and Coracle all repress postsynaptic GluRIIA accumulation and functional neurotransmission strength, but we still need a mechanistic link to the increase in presynaptic bouton formation via this pathway.

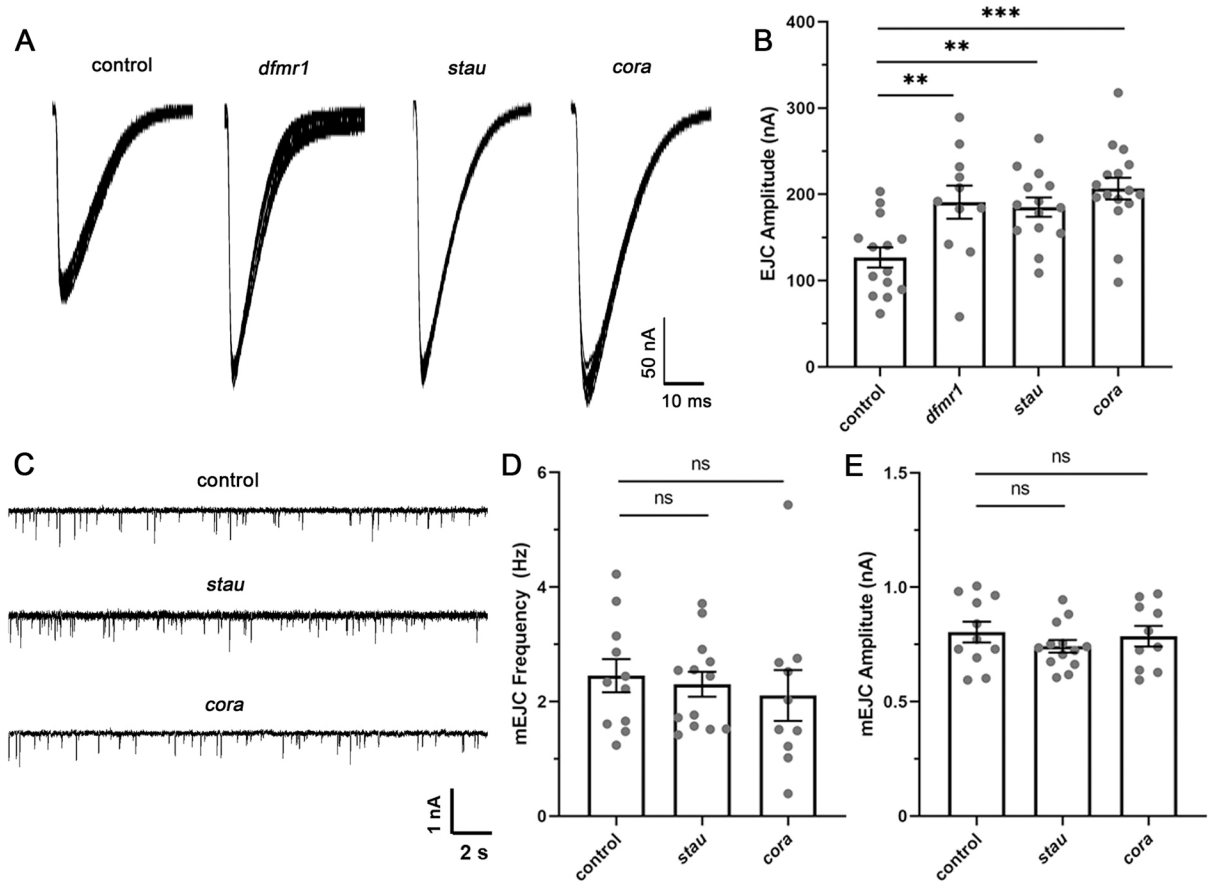


**Fig. 7. FMRP, Staufen and Coracle all negatively regulate NMJ transmission.** Two-electrode voltage-clamp recordings of synaptic function comparing genetic background control ($w^{1118}$) with *dfmr1* ($dfmr1^{50M}$), *staufen* ($stau^{HL}$) and coracle ($cora^{14}$) mutants. (A) Example motor nerve-stimulated evoked excitatory junctional current (EJC) traces (1.0 mM $Ca^{2+}$) showing ten superimposed responses in control (leftmost) versus *dfmr1*, *staufen* and *coracle* mutants. (B) Quantification of EJC amplitudes in all four genotypes. **$P$<0.01 and ***$P$<0.001. (C) Example miniature EJC (mEJC) recordings showing spontaneous synaptic vesicle fusion events. (D,E) Quantification of the overall mEJC frequency (D) and mEJC amplitude (E). There is no significant (ns) difference compared with the control for either measurement.

Development (2022) 149, dev200045. doi:10.1242/dev.200045

### FMRP, Staufen and Coracle all negatively regulate *trans*-synaptic pMad signaling

Functional GluRIIA accumulation in the *dfmr1* mutant induces presynaptic bouton development via a non-canonical BMP *trans*-synaptic signaling pathway (Sulkowski et al., 2016; Kamimura et al., 2019). This may not involve a BMP ligand, but rather a direct interaction between postsynaptic GluRIIA and presynaptic BMP receptor (Sulkowski et al., 2016). Intercellular signaling triggers synaptic phosphorylation of pMad to induce bouton formation (Kamimura et al., 2019; Sulkowski et al., 2016; Upadhyay et al., 2017). As *dfmr1*, *staufen* and *coracle* mutants all showed increased GluRIIA levels and bouton formation, we hypothesized that all mutants activate GluRIIA-dependent signaling of presynaptic pMad. To test this idea, we triple labeled all three mutants with anti-HRP (to mark neuronal presynaptic membrane), anti-Bruchpilot (Brp; to mark presynaptic active zones) and anti-pMad (Kamimura et al., 2019). The Brp-positive active zones and pMad levels were assayed within anti-HRP thresholded boutons using laser-scanning confocal microscopy (LSM). However, this approach has restricted X-Y resolution to visualize the small, closely spaced active zones (~500-600 nm diameter; Guggenheim et al., 2016; Pielage et al., 2006; Wegel et al., 2016). Therefore, to better resolve pMad around Brp puncta, we also used higher resolution structured illumination microscopy (SIM) (Guggenheim et al., 2016).

In LSM imaging, Brp-positive active zone numbers in *dfmr1*, *staufen* and *coracle* mutant NMJs were all comparable to those in control NMJs, whereas the surrounding pMad labeling was consistently elevated in all three mutants (Fig. 8A). Note that Brp did not colocalize with pMad, indicating that pMad surrounds the presynaptic active zones but is not present within each synapse. Compared with genetic control ($w^{1118}$) normalized pMad levels (intensity: 1.00±0.061), fluorescence quantification showed that presynaptic pMad was significantly elevated in *dfmr1* (1.52±0.14; $P$=0.005), *staufen* (1.64±0.14; $P$=0.001) and *coracle* (1.78±0.14; $P$<0.0001) mutants (Fig. 8C). At higher resolution, SIM imaging clearly revealed elevated pMad levels surrounding presynaptic active zones in all *dfmr1*, *staufen* and *coracle* mutants compared with controls (Fig. 8B). Note in single NMJ boutons that Brp and pMad labeling was non-overlapping, but adjacent. In all three of the mutants, presynaptic pMad aberrantly accumulated around Brp-positive active zones. Importantly, quantification of the active zones compared with matched control (Brp puncta density/μm$^2$: 1.44±0.07) showed no significant change in the *coracle* (1.54±0.05; $P$=0.54), *staufen* (1.46±0.02; $P$=0.99) or *dfmr1* (1.63±0.11; $P$=0.11) mutants (Fig. 8D). These findings suggest that elevated pMad levels in all three mutants correlate with increased GluRIIA-dependent retrograde *trans*-synaptic signaling from the postsynaptic domain, rather than presynaptic active zone density.

To directly test the postsynaptic to presynaptic signaling mechanism, all three genes were knocked down with muscle-targeted RNAi (Fig. S6). Compared with the driver control (24B-Gal4/+), postsynaptic *dfmr1* RNAi caused a clear and consistent increase in presynaptic pMad levels (Fig. S6A). Quantification normalized to the control showed a significant

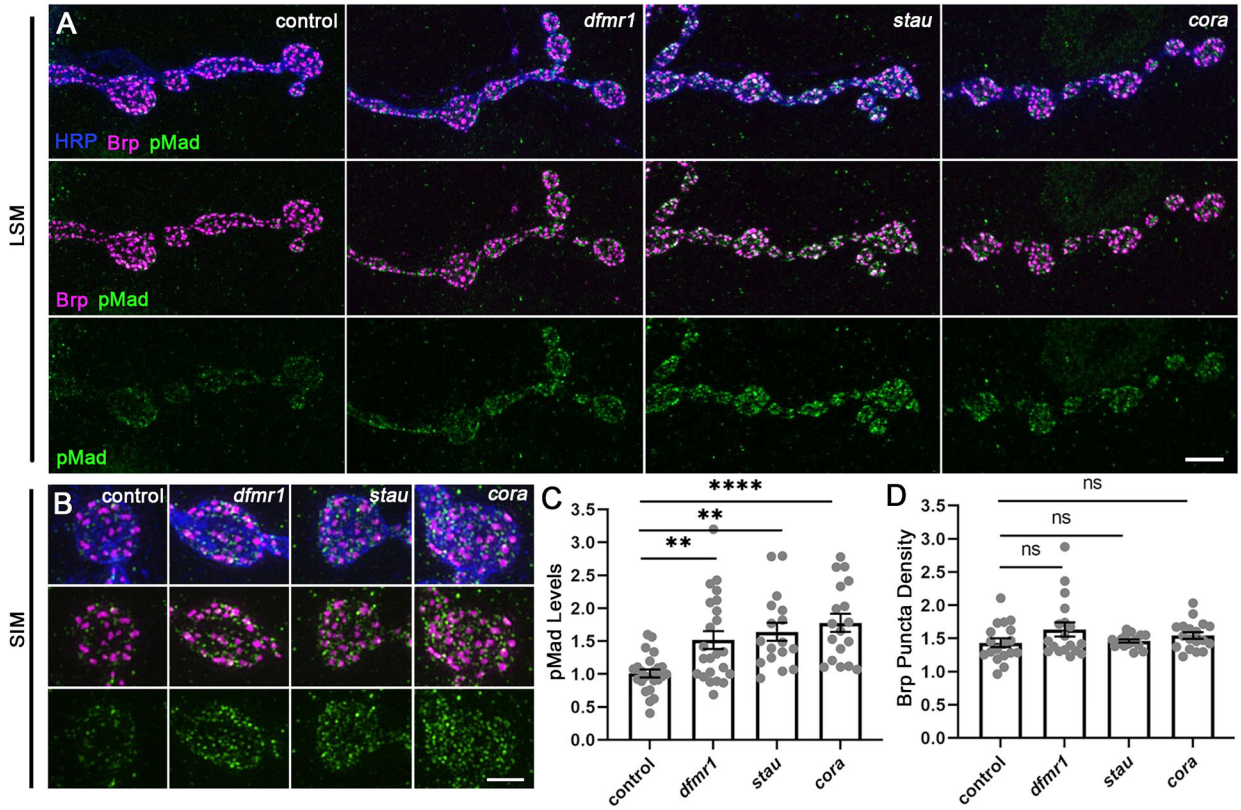


**Fig. 8. FMRP, Staufen and Coracle all negatively regulate NMJ pMad signaling.** Larval NMJs labeled for phosphorylated Mothers against decapentaplegic (pMad) at presynaptic active zones comparing genetic background control ($w^{1118}$) with *dfmr1* (*dfmr1*$^{50M}$), *staufen* (*stau*$^{HL}$) and *coracle* (*cora*$^{14}$) mutants. (A) Laser scanning confocal microscope triple labeling for HRP (blue), active zone Bruchpilot (Brp; magenta) and pMad (green), with overlap shown in white. (B) Higher-resolution structured illumination microscope imaging of single synaptic boutons. (C) Quantification of pMad fluorescence intensity normalized to the background control. **$P$<0.01 and ****$P$<0.0001. (D) Quantification of synapse density (Brp puncta active zone number per μm$^2$). There is no significant (ns) difference compared with the control for any of the mutants. Scale bars: 5 μm (A); 2 μm (B).

Development (2022) 149, dev200045. doi:10.1242/dev.200045

elevation in the knockdown (control 1.00±0.086, *dfmr1* RNAi 1.40±0.12; $P$=0.0098), with no change in BRP-marked active zone density ($P$=0.85; Fig. S6B). Similarly, targeted knockdown of postsynaptic *staufen* resulted in an obvious elevation in pMad levels (Fig. S6C). Quantification again indicated a significant increase in pMad fluorescence (control 1.00±0.085, *stau* RNAi 1.44±0.13; $P$=0.0072), with no change in synapse number ($P$=0.78; Fig. S6D). Finally, muscle-targeted *coracle* RNAi also drove heightened presynaptic pMad levels (Fig. S6E). Quantification likewise showed that there is a significant increase in pMad in the presynaptic boutons (control 1.00±0.084, *cora* RNAi 1.28±0.10, $P$=0.049), with no change in BRP-marked active zone density (Fig. S6F). These findings indicate that targeted loss of all three genes in the postsynaptic muscle causes *trans*-synaptic elevation of pMad surrounding neuronal presynaptic active zones. Taken together, these results suggest that accumulated postsynaptic GluRIIA in *dfmr1*, *staufen* and *coracle* mutants activates presynaptic pMad signaling, which in turn induces new bouton formation during NMJ synaptic development.

## DISCUSSION

This study reveals the mechanism of the established FMRP negative regulation of postsynaptic GluRIIA receptors and presynaptic bouton formation in the *Drosophila* FXS disease model (Pan and Broadie, 2007; Zhang et al., 2001). Specifically, the mRNA-binding FMRP-positive translational regulator binds to *staufen* mRNA as predicted (D'Annessa et al., 2019), within the postsynaptic cell. Consequently, both *dfmr1* and *staufen* mutants share the elevated GluRIIA level and bouton number phenotypes based on a common postsynaptic pathway function, and genetically interact as trans-heterozygotes to reproduce these phenotypes. Staufen acts as a dsRBP (Banerjee and Barraud, 2014) to bind *coracle* mRNA as predicted (Laver et al., 2013); both *dfmr1* and *staufen* mutants exhibit elevated postsynaptic Coracle levels, and genetically interact as trans-heterozygotes to reproduce this phenotype. Coracle acts as a GluRIIA-binding anchoring scaffold within the postsynaptic domain to regulate local receptor accumulation (Chen et al., 2005). Consequently, *dfmr1*, *staufen* and *coracle* mutants all increase NMJ synaptic functional differentiation to elevate neurotransmission strength. Finally, the elevated postsynaptic GluRIIA levels mediate retrograde BMP receptor *trans*-synaptic signaling that induces pMad to drive new presynaptic bouton development (Kamimura et al., 2019; Sulkowski et al., 2016). *dfmr1*, *staufen* and *coracle* mutants all exhibit elevated presynaptic pMad levels, thereby linking the postsynaptic GluRIIA accumulation and presynaptic supernumerary bouton formation defects shared by all of these mutants.

The *staufen* mutant increased synaptic Coracle levels, GluRIIA levels and bouton number are all internally consistent. In a previous study (Gardiol and St Johnston, 2014), opposite phenotypes were measured in $staufen^{HL}$/*Df(2R)Pcl7B*, which reduces another 14 genes in heterozygous deficiency, including loci involved in neuronal development (e.g. *grh*, *nopo*; Almeida and Bray, 2005; Bakshi et al., 2020; Ketosugbo et al., 2017; Merkle et al., 2009). Importantly, we similarly found reduced synaptic protein levels and bouton number in $staufen^{HL}$/*Df(2R)Pcl7B*, suggesting that heterozygosity of one or more of the neighboring genes impairs synaptic development (Mutsuddi et al., 2004; Tsou et al., 2015; Yilmazer et al., 2016). However, we showed that a *staufen* RNAi that reduces transcript levels by ∼90% replicates the *staufen* mutant NMJ phenotypes of increased GluRIIA levels and synaptic bouton numbers. We also replicated this with a second, independent *staufen* RNAi line. Moreover, we showed that the effect is entirely restricted to postsynaptic muscle RNAi, with no effect from presynaptic neuron RNAi, consistent with restricted postsynaptic Staufen function (Gardiol and St Johnston, 2014). In addition, postsynaptic *staufen* rescue of the *staufen* mutant restored normal synaptic bouton formation, with OE reducing GluRIIA levels in *staufen* mutants and rescuing GluRIIA levels in *dfmr1* mutants. Both *staufen* mutants and postsynaptic *staufen* RNAi also share the arrested supernumerary satellite bouton development characterizing *dfmr1* null mutants (Friedman et al., 2013). These many independent lines of evidence confirm our results, and are consistent with the known parallel FMRP role in restricting GluRIIA levels and synaptic bouton formation (Pan and Broadie, 2007; Zhang et al., 2001).

To regulate Staufen, FMRP binds *staufen* mRNA and protects targeted *staufen* transcripts from degradation. FMRP contains at least three distinct RNA-binding domains (RBDs) (Kenny and Ceman, 2016), and Staufen has five RBDs (Laver et al., 2013). Staufen reportedly binds a specific RNA hairpin structure formed by long 3′ UTRs (Gardiol and St Johnston, 2014; Laver et al., 2013), but our RIP shows that Staufen also binds mRNAs that are not predicted to generate this secondary structure (Ramos et al., 2000). Although the decreased *staufen* mRNA levels in both *dfmr1* mutants and muscle-targeted *dfmr1* RNAi are predicted to be due to the lack of FMRP binding, it is also possible that other unregulated interactors cause the downregulated *staufen* mRNA expression (Shah et al., 2020). Localized labeling with an anti-Staufen antibody has been reported in the postsynaptic NMJ (Gardiol and St Johnston, 2014), which we can confirm, but we could not reduce labeling in *staufen* hypomorphic mutants. We therefore have not shown Staufen labeling in the current study. Moreover, western blots have been reported with the same anti-Staufen antibody (St Johnston et al., 1991); however, our attempts were unsuccessful. We therefore used qPCR to measure *staufen* mRNA levels. Staufen binds to *coracle* mRNA, but does so in a non-selective manner. This result is consistent with Staufen acting as a very broad spectrum dsRBP (Heraud-Farlow and Kiebler, 2014; Laver et al., 2013), and suggests that Staufen likely acts with a translational regulator partner to generate specificity. FMRP is very well established to partner with other RBPs to mediate the translational regulation of its target transcripts (Bardoni et al., 1999, 2003; Didiot et al., 2009; Kenny et al., 2014).

The postsynaptic Coracle scaffold acts in a GluRIIA local anchoring mechanism, presumably to link the receptors to the underlying actin cytoskeleton (Chen et al., 2005). The jointly elevated Coracle and GluRIIA levels in both *dfmr1* and *staufen* mutants are consistent with this scaffold function. Because the *dfmr1*/+; *staufen*/+ trans-heterozygotes share this correlated Coracle and GluRIIA upregulation in the postsynaptic domain, a single common signaling pathway is indicated. Coracle also restricts terminal branching development in peripheral sensory neurons (Jiang et al., 2019; Tenenbaum et al., 2017). Both *coracle* mutants and sensory neuron-targeted *coracle* RNAi also display increased dendritic branch and termini numbers. These phenotypes are similar to the expanded NMJ terminals and increased synaptic bouton development reported here. Importantly, both *coracle* loss of function (mutants and muscle-targeted RNAi) and gain of function (muscle-targeted OE) increase postsynaptic GluRIIA levels and generate supernumerary boutons. Likewise, the knockdown and OE of many other similar scaffolds are known to cause phenocopying defects (McCarthy, 2010). Some examples include the muscle chaperone UNC-45 (Landsverk et al., 2007), the tight junction scaffold zonula occludens-1 (ZO-1) (Tokuda et al., 2014) and

Development (2022) 149, dev200045. doi:10.1242/dev.200045

synaptic UNC-13 (Fulterer et al., 2018). Indeed, both *coracle* loss and OE similarly cause increased dendritic crossing in *Drosophila* sensory neurons (Tenenbaum et al., 2017), similar to the phenocopy of developmental defects reported here. Combining the roles of postsynaptic FMRP–Staufen–Coracle in GluRIIA clustering, we reasoned that this pathway must be a regulatory determinant of synaptic functional development.

Removing FMRP, Staufen and Coracle strongly enhances functional synaptic differentiation and NMJ neurotransmission strength. This is consistent with expectations from the postsynaptic GluRIIA accumulation in all of these mutants (Harris and Littleton, 2015). Elevated GluRIIA levels are well known to be associated with increased evoked functional responses and prolonged channel open times (DiAntonio et al., 1999; Schmid et al., 2008). A GluRIIA pore sequence (MQQ) critically required for the *Drosophila* channel $Ca^{2+}$ permeability is conserved in mammalian receptors (Petersen et al., 1997). This selectivity allows $Ca^{2+}$-dependent participation in spontaneous (mEJC) and evoked (EJC) neurotransmission (Han et al., 2015). Although enhanced evoked EJC amplitudes are typically accompanied by mEJC alterations (Karunanithi et al., 2020; Sandstrom, 2011; Tsurudome et al., 2010), we find that mEJC amplitude and frequency are unchanged in both the *staufen* and *coracle* mutants, and show only minimal changes in the *dfmr1* mutants (Zhang et al., 2001). Classically, both evoked and spontaneous neurotransmission were thought to be mediated by the same vesicles (del Castillo and Katz, 1954; Groemer and Klingauf, 2007); however, more recent evidence has indicated that spontaneous and evoked neurotransmission have distinct machinery and vesicle pools (Groffen et al., 2010; Horvath et al., 2020; Ramirez et al., 2012; Sara et al., 2005). Postsynaptic receptors can be segregated into different compartments that are activated by either spontaneous or evoked release (Atasoy et al., 2008). Our work supports this growing body of evidence for differential regulation. Importantly, GluRIIA has unique functions, modulating both presynaptic glutamate release and presynaptic bouton development (Bogdanik et al., 2004; Kamimura et al., 2019).

The *dfmr1*, *staufen* and *coracle* mutants all showed upregulated presynaptic pMad correlated with postsynaptic activated GluRIIA accumulation. GluRIIA activation triggers presynaptic pMad signaling via BMP receptors surrounding active zones, which, in turn, stabilizes GluRIIA receptors in the postsynaptic domains (Sulkowski et al., 2016). This *trans*-synaptic signaling mechanism induces new presynaptic bouton development. The targeted postsynaptic RNAi for all three genes confirms this intercellular link. Synaptic BMP signaling involves both the type I serine/threonine kinase receptors and the type II receptor Wit (Upadhyay et al., 2017). Although BMP ligand Glass bottom boat (Gbb) signaling via Wit presynaptic receptors is well established at the NMJ to modulate synaptogenesis (Ellis et al., 2010; Kim et al., 2019; McCabe et al., 2003), the mechanism of presynaptic bouton formation induced by activated GluRIIA signaling does not involve canonical BMP signaling via Gbb (Friedman et al., 2013; Kamimura et al., 2019). In the *dfmr1* mutants, we suggest that postsynaptic GluRIIA accumulation induces presynaptic bouton development via non-canonical GluRIIA-Wit *trans*-synaptic retrograde signaling (Sulkowski et al., 2016). Similarly, the muscle postsynaptic glypican Dally-like protein (Dlp) (Kamimura and Maeda, 2021) negatively regulates NMJ synaptic development by inhibiting this same non-canonical BMP pathway through decreased activated GluRIIA expression (Kamimura et al., 2019). Postsynaptic GluRIIA clustering can thus trigger presynaptic bouton formation, although supernumerary boutons do not always induce reciprocal GluRIIA changes (Sulkowski et al., 2016). We conclude that an FMRP–Staufen–Coracle–GluRIIA–pMad pathway regulates intertwined structural and functional glutamatergic synapse development.

## MATERIALS AND METHODS

### *Drosophila* genetics

All stocks were reared at 25°C on standard cornmeal/agar/molasses food. The genetic background control was $w^{1118}$. The viable *dfmr1* mutant was *w*; $dfmr1^{50M}$, in which the *dfmr1* locus has been completely removed via a P-element imprecise excision deletion (Zhang et al., 2001). The larval viable *staufen* mutant was *w*; $stau^{HL}$, which has a point mutation in the dsRNA-binding domain 5 specifically required for local mRNA translation (Fig. S1A; St Johnston et al., 1991). The viable *coracle* mutant was *w*; $cora^{14}$, which has a nonsense mutation ($Arg^{1607}$) reducing function (Lamb et al., 1998; Ward et al., 2001). Transgenic drivers were ubiquitous *daughterless* UH1-Gal4 (Rohrbough et al., 2004), neuronal *elav*-Gal4 (Kan et al., 2021) and muscle-specific 24B-Gal4 (Kim et al., 2021). All genetic crosses and recombinations to make double mutant lines were done using standard approaches. Transgenic UAS lines used in this study are listed in Table S1.

### Antibody labeling

Staged wandering third instars were dissected in phosphate-buffered saline (PBS). For FMRP, DLG, Brp and pMad labeling, tissues were fixed in 4% paraformaldehyde (PFA) diluted in PBS for 10 min at room temperature (RT). Coracle labeling was performed with 20 min fixation at RT. To label GluRIIA, larvae were fixed in 100% Bouin's fixative (Karr et al., 2009) for 5 min at RT. Fixed preparations were blocked for 1 h at RT in PBS with 0.2% Triton X-100 (PBST) plus 1% bovine serum albumin (BSA). Primary antibody incubation was done overnight at 4°C and secondary antibody incubation was done for 2.5 h at RT. Primary antibodies used were as follows: mouse anti-DLG [Developmental Studies Hybridoma Bank (DSHB), 4F3, 1:50], mouse anti-GluRIIA (DSHB, 8B4D2, 1:50), mouse anti-Coracle (DSHB, C566.9, 1:50), mouse anti-FMRP (Abcam, 10299, 1:250), mouse anti-Brp (DSHB, NC82, 1:100), rabbit anti-Smad3 (phospho S423+S425, Abcam 52903, 1:500), Cy5-conjuagted goat anti-HRP (Jackson ImmunoResearch, 147967, 1:250) and Cy3-conjugated goat anti-HRP (Jackson ImmunoResearch, 137589, 1:250). Secondary antibodies used were as follows: goat 488 anti-mouse (Invitrogen, A11001, 1:250), goat 488 anti-rabbit (Invitrogen, A11008, 1:250), donkey 555 anti-mouse (Invitrogen, A31570, 1:250) and donkey 488 anti-mouse (Invitrogen, A21202, 1:250).

### Synaptic imaging

All confocal imaging was performed on a Zeiss LSM 510 META laser-scanning confocal microscope and projected in Zen software (Kopke et al., 2020). The NMJ areas and fluorescent intensities were analyzed via blinded *z*-stack sum projection in FIJI software (Guillen et al., 2020). GluRIIA levels were quantified in HRP-labeled NMJ areas with eliminated muscle intensity background, while Coracle levels were quantified in dilated 1 µm rings surrounding individual NMJ boutons. For SIM, samples were imaged on a Nikon N-SIM microscope in 3D SIM mode (Kopke et al., 2020). Fluorophores were activated by 647 nm, 561 nm and 488 nm diode lasers. With a SR Apo TIRF 100× oil objective (1.49 NA WD 0.12) and an Andor iXon Ultra DU-897 EMCCD monochrome camera, samples were reconstructed through NIS-Elements (Nikon) with 0.12 µm step-size stacks. Stack reconstructions of the blinded raw data were done before image rendering and measurement analyses.

### Quantitative real-time PCR

The total RNA from wandering third instars was isolated according to the instructions in the RNeasy Plus Mini Kit (Qiagen 74134). RNA (2 µg) measured by a Nanodrop 2000C was then reverse transcribed into complementary DNA (cDNA) with random hexamers using the High Capacity cDNA Reverse Transcription Kit (Applied Biosystems, 4368814).

Development (2022) 149, dev200045. doi:10.1242/dev.200045

Resulting single-strand cDNA was then subjected to real-time PCR employing the SYBR Green Master Mix (Applied Biosystems, A25742) and using the CFX384 Touch Real-Time PCR system (Bio-Rad). Targeted transcripts were normalized to reference gene cDNA (*GAPDH2*). The cDNA primers used in this study are listed in Table S2.

### RNA immunoprecipitation

Fifty wandering third instars of each genotype were homogenized in 500 µl RNase-free lysis buffer [20 mM HEPES, 100 mM NaCl, 2.5 mM EDTA, 0.05% (v/v) Triton X-100, 5% (v/v) glycerol] with 1% β-mercaptoethanol, 1× protease inhibitor cocktail (cOmplete mini EDTA-free Tablets, Sigma-Aldrich), and 400 U RNase inhibitor (Applied Biosystems, N8080119). To preclear the supernatant, the centrifuged lysates were incubated with 20 µl Protein G Dynabeads for 1 h at 4°C. In parallel, 200 µl Protein G Dynabeads were incubated in blocking buffer (1×PBS, 0.2% TWEEN 20, 0.1% tRNA and 5% BSA) for 1 h at 4°C, followed by coating with 10 µg of the primary antibody. Next, the precleared supernatant was incubated with antibody-bead conjugates overnight at 4°C. To reduce non-specific RNA binding in larval lysates, tRNA (Sigma-Aldrich, 10109541001) was added in lysis buffer as specified (e.g. 1 mg tRNA per 500 µl IP reaction). To purify bound RNAs, washed bead-protein-RNA complexes were incubated with a 500 µl TRIzole and chloroform mixture (Ambion, 15596026) for 10 min. Subsequently, 3 µl glycogen was applied to carry RNAs for the precipitation by mixing with 100 µl 2-propenol. The precipitated RNA was then reverse transcribed into single-strand cDNA and subjected to primer-specific PCR (Table S2). We used 2% agarose gels to analyze the PCR products. Primary antibodies used were mouse anti-Venus YFP (Sigma-Aldrich, MABE1906) and mouse anti-GFP (Sigma-Aldrich, G6539).

### Synaptic electrophysiology

Wandering third instars were dissected along the dorsal midline, internal organs were removed and body walls were glued down (Vetbond, 3 M). Next, all peripheral motor nerves were cut at the base of the ventral nerve cord. TEVC recordings were performed at 18°C in physiological saline (128 mM NaCl, 2 mM KCl, 4 mM $MgCl_2$, 1 mM $CaCl_2$, 70 mM sucrose and 5 mM HEPES, pH 7.2). Synaptic currents were recorded from ventral longitudinal muscle 6 of abdominal segments 3/4 under a Zeiss Axioskop microscope using a 40× water-immersion objective (Kopke et al., 2020). Muscles were impaled with two microelectrodes (1 mm outer diameter borosilicate capabilities; World Precision Instruments) of ∼15 MΩ resistance filled with 3 m KCl, and then clamped at a command voltage of −60 mV employing an Axoclamp-2B amplifier (Axon Instruments; Kopke et al., 2020). To make the EJC recordings, the motor nerve was stimulated using a fire-polished glass suction electrode with 0.5 ms suprathreshold voltage stimuli at 0.2 Hz (Grass S88 stimulator). Data were filtered at 2 kHz. To quantify EJC amplitude, ten consecutive traces were recorded and averaged, with the average peak amplitude being reported. Spontaneous mEJC events were recorded in continuous 2 min sessions at 10 kHz, and analyzed using a 200 Hz low-pass filter (Kopke et al., 2020). Clampex 9.0 was used for data acquisition, and Clampfit 9 was used for data analysis (Axon Instruments).

### Statistical analyses

All statistics were performed using GraphPad Prism software (v8.0). All data sets were subject to ROUT outlier tests with Q set to 1%. All paired data comparisons (i.e. bouton numbers, GluRIIA levels, FMRP levels, Coracle levels and qPCR measurements) were assayed using unpaired two-tailed Student's *t*-tests for two-way comparison with 95% confidence. All data sets of more than two comparisons (i.e. electrophysiology results, pMad levels and active zone numbers) were analyzed using one-way ANOVA. Dunnett's multiple comparison tests were performed to compare the mean of each experimental data set with the control mean. All figures show mean±s.e.m., with $P \leq 0.05$ considered significant.

#### Acknowledgements

We are grateful to the BDSC (Indiana University, Bloomington, IN, USA) and the VDRC (Vienna, Austria) for essential genetic lines, and the DSHB (University of Iowa, Iowa City, IA, USA) for essential antibodies. We thank Daniel St Johnston (The Gurdon Institute, University of Cambridge, Cambridge, UK) and Richard Fehon (University of Chicago, Chicago, IL, USA) for *staufen* and *coracle* stocks, respectively. We thank Julian Hillyer, He Huang and Jim Patton (Vanderbilt University, Nashville, TN, USA) for qPCR equipment use, qPCR advice and RIP advice, respectively. We thank the Broadie Laboratory for extensive input.

#### Competing interests

The authors declare no competing or financial interests.

#### Author contributions

Conceptualization: C.S., K.B.; Methodology: C.S., E.M.R.; Validation: C.S., K.B.; Formal analysis: C.S.; Investigation: C.S., S.N.L., E.M.R.; Resources: K.B.; Data curation: C.S.; Writing - original draft: C.S.; Writing - review & editing: C.S., S.N.L., K.B.; Visualization: C.S.; Supervision: K.B.; Project administration: K.B.; Funding acquisition: K.B.

#### Funding

This work was supported by funding from the National Institute of Mental Health (R01 grant MH084989 to K.B.). Deposited in PMC for release after 12 months.

#### References

**Almeida, M. S. and Bray, S. J.** (2005). Regulation of post-embryonic neuroblasts by *Drosophila* Grainyhead. *Mech. Dev.* **122**, 1282-1293. doi:10.1016/j.mod.2005.08.004

**Atasoy, D., Ertunc, M., Moulder, K. L., Blackwell, J., Chung, C., Su, J. and Kavalali, E. T.** (2008). Spontaneous and evoked glutamate release activates two populations of NMDA receptors with limited overlap. *J. Neurosci.* **28**, 10151-10166. doi:10.1523/JNEUROSCI.2432-08.2008

**Bakshi, A., Sipani, R., Ghosh, N. and Joshi, R.** (2020). Sequential activation of Notch and Grainyhead gives apoptotic competence to abdominal-B expressing larval neuroblasts in *Drosophila* central nervous system. *PLoS Genet.* **16**, e1008976. doi:10.1371/journal.pgen.1008976

**Banerjee, S. and Barraud, P.** (2014). Functions of double-stranded RNA-binding domains in nucleocytoplasmic transport. *RNA Biol.* **11**, 1226-1232. doi:10.4161/15476286.2014.972856

**Barbee, S. A., Estes, P. S., Cziko, A.-M., Hillebrand, J., Luedeman, R. A., Coller, J. M., Johnson, N., Howlett, I. C., Geng, C., Ueda, R. et al.** (2006). Staufen-and FMRP-containing neuronal RNPs are structurally and functionally related to somatic P bodies. *Neuron* **52**, 997-1009. doi:10.1016/j.neuron.2006.10.028

**Bardoni, B., Schenck, A. and Louis Mandel, J.** (1999). A novel RNA-binding nuclear protein that interacts with the Fragile X Mental Retardation (FMR1) protein. *Hum. Mol. Genet.* **8**, 2557-2566. doi:10.1093/hmg/8.13.2557

**Bardoni, B., Castets, M., Huot, M. E., Schenck, A., Adinolfi, S., Corbin, F., Pastore, A., Khandjian, E. W. and Mandel, J. L.** (2003). 82-FIP, a novel FMRP (Fragile X Mental Retardation Protein) interacting protein, shows a cell cycle-dependent intracellular localization. *Hum. Mol. Genet.* **12**, 1689-1698. doi:10.1093/hmg/ddg181

**Blackwell, E. and Ceman, S.** (2011). A new regulatory function of the region proximal to the RGG box in the Fragile X mental retardation protein. *J. Cell. Sci.* **124**, 3060-3065. doi:10.1242/jcs.086751

**Bogdanik, L., Mohrmann, R., Ramaekers, A., Bockaert, J., Grau, Y., Broadie, K. and Parmentier, M. L.** (2004). The *Drosophila* metabotropic glutamate receptor DmGluRA regulates activity-dependent synaptic facilitation and fine synaptic morphology. *J. Neurosci.* **24**, 9105-9116. doi:10.1523/JNEUROSCI.2724-04.2004

**Bolduc, F. V., Bell, K., Cox, H., Broadie, K. and Tully, T.** (2008). Excess protein synthesis in *Drosophila* Fragile X mutants impairs long-term memory. *Nat. Neurosci.* **11**, 1143-1145. doi:10.1038/nn.2175

**Bonnet-Magnaval, F.** (2016). Hypoxia and ER stress promote Staufen1 expression through an alternative translation mechanism. *Biochem. Biophys. Res. Commun.* **479**, 365-371. doi:10.1016/j.bbrc.2016.09.082

**Chen, K., Merino, C., Sigrist, S. J. and Featherstone, D. E.** (2005). The 4.1 protein coracle mediates subunit-selective anchoring of *Drosophila* glutamate receptors to the postsynaptic actin cytoskeleton. *J. Neurosci.* **25**, 6667-6675. doi:10.1523/JNEUROSCI.1527-05.2005

**Chou, V. T., Johnson, S. A. and Van Vactor, D.** (2020). Synapse development and maturation at the *Drosophila* neuromuscular junction. *Neural Dev.* **15**, 11. doi:10.1186/s13064-020-00147-5

**Chu, J.-F., Majumder, P., Chatterjee, B., Huang, S. L. and Shen, C. K. J.** (2019). TDP-43 regulates coupled dendritic mRNA transport-translation processes in co-operation with FMRP and Staufen1. *Cell Rep.* **29**, 3118-3133.e6. doi:10.1016/j.celrep.2019.10.061

**Clarke, G. L., Chen, J. and Nishimune, H.** (2012). Presynaptic active zone density during development and synaptic plasticity. *Front. Mol. Neurosci.* **5**, 12. doi:10.3389/fnmol.2012.00012

**Comery, T. A., Harris, J. B., Willems, P. J., Oostra, B. A., Irwin, S. A., Weiler, I. J. and Greenough, W. T.** (1997). Abnormal dendritic spines in Fragile X knockout

mice: maturation and pruningdeficits. *Proc. Natl Acad. Sci. USA* **94**, 5401-5404. doi:10.1073/pnas.94.10.5401

**Connor, S. A., Hoeffer, C. A., Klann, E. and Nguyen, P. V.** (2011). Fragile X mental retardation protein regulates heterosynaptic plasticity in the hippocampus. *Learn. Mem.* **18**, 207-220. doi:10.1101/lm.2043811

**Crawford, D. C., Acuña, J. M. and Sherman, S. L.** (2001). *FMR1* and the Fragile X Syndrome: human genome epidemiology review. *Genet. Med.* **3**, 359-371. doi:10.1097/00125817-200109000-00006

**Cziko, A.-M. J., McCann, C. T., Howlett, I. C., Barbee, S. A., Duncan, R. P., Luedemann, R., Zarnescu, D., Zinsmaier, K. E., Parker, R. R. and Ramaswami, M.** (2009). Genetic modifiers of *dFMR1* encode RNA granule components in *Drosophila*. *Genetics* **182**, 1051-1060. doi:10.1534/genetics.109.103234

**D'Annessa, I., Cicconardi, F. and Di Marino, D.** (2019). Handling FMRP and its molecular partners: structural insights into Fragile X Syndrome. *Prog. Biophys. Mol. Biol.* **141**, 3-14. doi:10.1016/j.pbiomolbio.2018.07.001

**del Castillo, J. and Katz, B.** (1954). Quantal components of the end-plate potential. *J. Physiol.* **124**, 560-573. doi:10.1113/jphysiol.1954.sp005129

**DiAntonio, A., Petersen, S. A., Heckmann, M. and Goodman, C. S.** (1999). Glutamate receptor expression regulates quantal size and quantal content at the *Drosophila* neuromuscular junction. *J. Neurosci.* **19**, 3023-3032. doi:10.1523/JNEUROSCI.19-08-03023.1999

**Didiot, M.-C., Subramanian, M., Flatter, E., Mandel, J.-L. and Moine, H.** (2009). Cells lacking the Fragile X mental retardation protein (FMRP) have normal RISC activity but exhibit altered stress granule assembly. *MBoC* **20**, 428-437. doi:10.1091/mbc.e08-07-0737

**Drozd, M., Bardoni, B. and Capovilla, M.** (2018). Modeling Fragile X Syndrome in *Drosophila*. *Front. Mol. Neurosci.* **11**, 124. doi:10.3389/fnmol.2018.00124

**Dugré-Brisson, S., Elvira, G., Boulay, K., Chatel-Chaix, L., Mouland, A. J. and DesGroseillers, L.** (2005). Interaction of Staufen1 with the 5′ end of mRNA facilitates translation of these RNAs. *Nucleic Acids Res.* **33**, 4797-4812. doi:10.1093/nar/gki794

**Ellis, J. E., Parker, L., Cho, J. and Arora, K.** (2010). Activin signaling functions upstream of Gbb to regulate synaptic growth at the *Drosophila* neuromuscular junction. *Dev. Biol.* **342**, 121-133. doi:10.1016/j.ydbio.2010.03.012

**Flockhart, I., Booker, M., Kiger, A., Boutros, M., Armknecht, S., Ramadan, N., Richardson, K., Xu, A., Perrimon, N. and Mathey-Prevot, B.** (2006). FlyRNAi: the *Drosophila* RNAi screening center database. *Nucleic Acids Res.* **34**, D489-D494. doi:10.1093/nar/gkj114

**Friedman, S. H., Dani, N., Rushton, E. and Broadie, K.** (2013). Fragile X mental retardation protein regulates trans-synaptic signaling in *Drosophila*. *Dis. Model. Mech.* **6**, 1400-1413. doi:10.1242/dmm.012229

**Fulterer, A., Andlauer, T. F. M., Ender, A., Maglione, M., Eyring, K., Woitkuhn, J., Lehmann, M., Matkovic-Rachid, T., Geiger, J. R. P., Walter, A. M. et al.** (2018). Active zone scaffold protein ratios tune functional diversity across brain synapses. *Cell Rep.* **23**, 1259-1274. doi:10.1016/j.celrep.2018.03.126

**Furic, L., Maher-Laporte, M. and DesGroseillers, L.** (2008). A genome-wide approach identifies distinct but overlapping subsets of cellular mRNAs associated with Staufen1- and Staufen2-containing ribonucleoprotein complexes. *RNA* **14**, 324-335. doi:10.1261/rna.720308

**Garber, K. B., Visootsak, J. and Warren, S. T.** (2008). Fragile X Syndrome. *Eur. J. Hum. Genet.* **16**, 666-672. doi:10.1038/ejhg.2008.61

**Gardiol, A. and St Johnston, D.** (2014). Staufen targets *coracle* mRNA to *Drosophila* neuromuscular junctions and regulates GluRIIA synaptic accumulation and bouton number. *Dev. Biol.* **392**, 153-167. doi:10.1016/j.ydbio.2014.06.007

**Gomez, J. M., Wang, Y. and Riechmann, V.** (2012). Tao controls epithelial morphogenesis by promoting Fasciclin 2 endocytosis. *J. Cell. Biol.* **199**, 1131-1143. doi:10.1083/jcb.201207150

**Groemer, T. W. and Klingauf, J.** (2007). Synaptic vesicles recycling spontaneously and during activity belong to the same vesicle pool. *Nat. Neurosci.* **10**, 145-147. doi:10.1038/nn1831

**Groffen, A. J., Martens, S., Díez Arazola, R., Cornelisse, L. N., Lozovaya, N., de Jong, A. P. H., Goriounova, N. A., Habets, R. L. P., Takai, Y., Borst, J. G. et al.** (2010). Doc2b is a high-affinity $Ca^{2+}$ sensor for spontaneous neurotransmitter release. *Science* **327**, 1614-1618. doi:10.1126/science.1183765

**Guggenheim, E. J., Khan, A., Pike, J., Chang, L., Lynch, I. and Rappoport, J. Z.** (2016). Comparison of confocal and super-resolution reflectance imaging of metal oxide nanoparticles. *PLoS One* **11**, e0159980. doi:10.1371/journal.pone.0159980

**Guillen, R. X., Beckley, J. R., Chen, J.-S. and Gould, K. L.** (2020). CRISPR-mediated gene targeting of CK1δ/ε leads to enhanced understanding of their role in endocytosis via phosphoregulation of GAPVD1. *Sci. Rep.* **10**, 6797. doi:10.1038/s41598-020-63669-2

**Han, T. H., Dharkar, P., Mayer, M. L. and Serpe, M.** (2015). Functional reconstitution of *Drosophila* melanogaster NMJ glutamate receptors. *Proc. Natl Acad. Sci. USA* **112**, 6182-6187. doi:10.1073/pnas.1500458112

**Hansen, R. S., Gartler, S. M., Scott, C. R., Chen, S. H. and Laird, C. D.** (1992). Methylation analysis of CGG sites in the CpG island of the human *FMR1* gene. *Hum. Mol. Genet.* **1**, 571-578. doi:10.1093/hmg/1.8.571

**Harris, K. P. and Littleton, J. T.** (2015). Transmission, development, and plasticity of synapses. *Genetics* **201**, 345-375. doi:10.1534/genetics.115.176529

**Heraud-Farlow, J. E. and Kiebler, M. A.** (2014). The multifunctional Staufen proteins: conserved roles from neurogenesis to synaptic plasticity. *Trends Neurosci.* **37**, 470-479. doi:10.1016/j.tins.2014.05.009

**Hong, H., Zhao, K., Huang, S., Huang, S., Yao, A., Jiang, Y., Sigrist, S., Zhao, L. and Zhang, Y. Q.** (2020). Structural remodeling of active zones is associated with synaptic homeostasis. *J. Neurosci.* **40**, 2817-2827. doi:10.1523/JNEUROSCI.2002-19.2020

**Horvath, P. M., Piazza, M. K., Monteggia, L. M. and Kavalali, E. T.** (2020). Spontaneous and evoked neurotransmission are partially segregated at inhibitory synapses. *eLife* **9**, e52852. doi:10.7554/eLife.52852

**Jan, L. Y. and Jan, Y. N.** (1982). Antibodies to horseradish peroxidase as specific neuronal markers in *Drosophila* and in grasshopper embryos. *Proc. Natl Acad. Sci. USA* **79**, 2700-2704. doi:10.1073/pnas.79.8.2700

**Jiang, N., Rasmussen, J. P., Clanton, J. A., Rosenberg, M. F., Luedke, K. P., Cronan, M. R., Parker, E. D., Kim, H.-J., Vaughan, J. C., Sagasti, A. et al.** (2019). A conserved morphogenetic mechanism for epidermal ensheathment of nociceptive sensory neurites. *eLife* **8**, e42455. doi:10.7554/eLife.42455

**Kamimura, K. and Maeda, N.** (2021). Glypicans and heparan sulfate in synaptic development, neural plasticity, and neurological disorders. *Front. Neural Circuits* **15**, 595596. doi:10.3389/fncir.2021.595596

**Kamimura, K., Odajima, A., Ikegawa, Y., Maru, C. and Maeda, N.** (2019). The HSPG Glypican regulates experience-dependent synaptic and behavioral plasticity by modulating the non-canonical BMP pathway. *Cell Rep.* **28**, 3144-3156.e4. doi:10.1016/j.celrep.2019.08.032

**Kan, L., Ott, S., Joseph, B., Park, E. S., Dai, W., Kleiner, R. E., Claridge-Chang, A. and Lai, E. C.** (2021). A neural $m^6A$/Ythdf pathway is required for learning and memory in *Drosophila*. *Nat. Commun.* **12**, 1458. doi:10.1038/s41467-021-21537-1

**Karr, J., Vagin, V., Chen, K., Ganesan, S., Olenkina, O., Gvozdev, V. and Featherstone, D. E.** (2009). Regulation of glutamate receptor subunit availability by microRNAs. *J. Cell Biol.* **185**, 685-697. doi:10.1083/jcb.200902062

**Karunanithi, S., Cylinder, D., Ertekin, D., Zalucki, O. H., Marin, L., Lavidis, N. A., Atwood, H. L. and Swinderen, B.** (2020). Proportional downscaling of glutamatergic release sites by the general anesthetic propofol at *Drosophila* motor nerve terminals. *eNeuro* **7**, ENEURO.0422-19.2020. doi:10.1523/ENEURO.0422-19.2020

**Kavalali, E. T.** (2015). The mechanisms and functions of spontaneous neurotransmitter release. *Nat. Rev. Neurosci.* **16**, 5-16. doi:10.1038/nrn3875

**Kenny, P. and Ceman, S.** (2016). RNA secondary structure modulates FMRP's bi-functional role in the MicroRNA pathway. *Int. J. Mol. Sci.* **17**, 985. doi:10.3390/ijms17060985

**Kenny, P. J., Zhou, H., Kim, M., Skariah, G., Khetani, R. S., Drnevich, J., Arcila, M. L., Kosik, K. S. and Ceman, S.** (2014). MOV10 and FMRP regulate AGO2 association with microRNA recognition elements. *Cell Rep.* **9**, 1729-1741. doi:10.1016/j.celrep.2014.10.054

**Kenny, P. J., Kim, M., Skariah, G., Nielsen, J., Lannom, M. C. and Ceman, S.** (2020). The FMRP–MOV10 complex: a translational regulatory switch modulated by G-Quadruplexes. *Nucleic Acids Res.* **48**, 862-878. doi:10.1093/nar/gkz1092

**Ketosugbo, K. F., Bushnell, H. L. and Johnson, R. I.** (2017). A screen for E3 ubiquitination ligases that genetically interact with the adaptor protein Cindr during *Drosophila* eye patterning. *PLoS One* **12**, e0187571. doi:10.1371/journal.pone.0187571

**Khadilkar, R. J., Vogl, W., Goodwin, K. and Tanentzapf, G.** (2017). Modulation of occluding junctions alters the hematopoietic niche to trigger immune activation. *eLife* **6**, e28081. doi:10.7554/eLife.28081

**Kim, N., Kim, S., Nahm, M., Kopke, D., Kim, J., Cho, E., Lee, M. J., Lee, M., Kim, S. H., Broadie, K. et al.** (2019). BMP-dependent synaptic development requires Abi-Abl-Rac signaling of BMP receptor macropinocytosis. *Nat. Commun.* **10**, 684. doi:10.1038/s41467-019-08533-2

**Kim, J., Kim, S., Nahm, M., Li, T. N., Lin, H. C., Kim, Y. D., Lee, J., Yao, C. K. and Lee, S.** (2021). ALS2 regulates endosomal trafficking, postsynaptic development, and neuronal survival. *J. Cell Biol.* **220**, e202007112. doi:10.1083/jcb.202007112

**Kopke, D. L., Leahy, S. N., Vita, D. J., Lima, S. C., Newman, Z. L. and Broadie, K.** (2020). Carrier of Wingless (Cow) regulation of *Drosophila* neuromuscular junction development. *eNeuro* **7**, ENEURO.0285-19.2020. doi:10.1523/ENEURO.0285-19.2020

**Lamb, R. S., Ward, R. E., Schweizer, L. and Fehon, R. G.** (1998). *Drosophila* Coracle, a member of the protein 4.1 superfamily, has essential structural functions in the septate junctions and developmental functions in embryonic and adult epithelial cells. *Mol. Biol. Cell* **9**, 3505-3519. doi:10.1091/mbc.9.12.3505

**Landskron, L., Steinmann, V., Bonnay, F., Burkard, T. R., Steinmann, J., Reichardt, I., Harzer, H., Laurenson, A. S., Reichert, H. and Knoblich, J. A.** (2018). The asymmetrically segregating lncRNA cherub is required for transforming stem cells into malignant cells. *eLife* **7**, e31347. doi:10.7554/eLife.31347

**Landsverk, M. L., Li, S., Hutagalung, A. H., Najafov, A., Hoppe, T., Barral, J. M. and Epstein, H. F.** (2007). The UNC-45 chaperone mediates sarcomere assembly through myosin degradation in *Caenorhabditis elegans*. *J. Cell Biol.* **177**, 205-210. doi:10.1083/jcb.200607084

**Laver, J. D., Li, X., Ancevicius, K., Westwood, J. T., Smibert, C. A., Morris, Q. D. and Lipshitz, H. D.** (2013). Genome-wide analysis of Staufen-associated mRNAs identifies secondary structures that confer target specificity. *Nucleic Acids Res.* **41**, 9438-9460. doi:10.1093/nar/gkt702

**Liu, B., Li, Y., Stackpole, E. E., Novak, A., Gao, Y., Zhao, Y., Zhao, X. and Richter, J. D.** (2018). Regulatory discrimination of mRNAs by FMRP controls mouse adult neural stem cell differentiation. *Proc. Natl Acad. Sci. USA* **115**, E11397-E11405. doi:10.1073/pnas.1809588115

**Marrus, S. B.** (2004). Differential localization of glutamate receptor subunits at the *Drosophila* neuromuscular junction. *J. Neurosci.* **24**, 1406-1415. doi:10.1523/JNEUROSCI.1575-03.2004

**McCabe, B. D., Marqués, G., Haghighi, A. P., Fetter, R. D., Crotty, M. L., Haerry, T. E., Goodman, C. S. and O'Connor, M. B.** (2003). The BMP homolog Gbb provides a retrograde signal that regulates synaptic growth at the *Drosophila* neuromuscular junction. *Neuron* **39**, 241-254. doi:10.1016/S0896-6273(03)00426-4

**McCarthy, N.** (2010). Regulation and crosstalk. *Nat. Rev. Mol. Cell Biol.* **11**, 390. doi:10.1038/nrm2915

**McClatchey, A. I.** (2012). ERM proteins. *Curr. Biol.* **22**, R784-R785. doi:10.1016/j.cub.2012.07.057

**Menon, K. P., Carrillo, R. A. and Zinn, K.** (2013). Development and plasticity of the *Drosophila* larval neuromuscular junction. *Wiley Interdiscip. Rev. Dev. Biol.* **2**, 647-670. doi:10.1002/wdev.108

**Merkle, J. A., Rickmyre, J. L., Garg, A., Loggins, E. B., Jodoin, J. N., Lee, E., Wu, L. P. and Lee, L. A.** (2009). no poles encodes a predicted E3 ubiquitin ligase required for early embryonic development of *Drosophila*. *Dev.* **136**, 449-459. doi:10.1242/dev.027599

**Micklem, D. R., Adams, J., Grünert, S. and St Johnston, D.** (2000). Distinct roles of two conserved Staufen domains in *oskar* mRNA localization and translation. *EMBO J.* **19**, 1366-1377. doi:10.1093/emboj/19.6.1366

**Müller, M. and Davis, G. W.** (2012). Transsynaptic control of presynaptic $Ca^{2+}$ influx achieves homeostatic potentiation of neurotransmitter release. *Curr. Biol.* **22**, 1102-1108. doi:10.1016/j.cub.2012.04.018

**Mutsuddi, M., Marshall, C. M., Benzow, K. A., Koob, M. D. and Rebay, I.** (2004). The spinocerebellar ataxia 8 noncoding RNA causes neurodegeneration and associates with Staufen in *Drosophila*. *Curr. Biol.* **14**, 302-308. doi:10.1016/j.cub.2004.01.034

**Myrick, L. K., Hashimoto, H., Cheng, X. and Warren, S. T.** (2015). Human FMRP contains an integral tandem Agenet (Tudor) and KH motif in the amino terminal domain. *Hum. Mol. Genet.* **24**, 1733-1740. doi:10.1093/hmg/ddu586

**Nagai, T., Ibata, K., Park, E. S., Kubota, M., Mikoshiba, K. and Miyawaki, A.** (2002). A variant of yellow fluorescent protein with fast and efficient maturation for cell-biological applications. *Nat. Biotechnol.* **20**, 87-90. doi:10.1038/nbt0102-87

**Pan, L. and Broadie, K. S.** (2007). *Drosophila* Fragile X mental retardation protein and metabotropic glutamate receptor A convergently regulate the synaptic ratio of ionotropic glutamate receptor subclasses. *J. Neurosci.* **27**, 12378-12389. doi:10.1523/JNEUROSCI.2970-07.2007

**Park, E. and Maquat, L. E.** (2013). Staufen-mediated mRNA decay. *WIREs RNA* **4**, 423-435. doi:10.1002/wrna.1168

**Petersen, S. A., Fetter, R. D., Noordermeer, J. N., Goodman, C. S. and DiAntonio, A.** (1997). Genetic analysis of glutamate receptors in *Drosophila* reveals a retrograde signal regulating presynaptic transmitter release. *Neuron* **19**, 1237-1248. doi:10.1016/S0896-6273(00)80415-8

**Petzoldt, A. G., Lee, Y. H., Khorramshahi, O., Reynolds, E., Plested, A. J. R., Herzel, H. and Sigrist, S. J.** (2014). Gating characteristics control glutamate receptor distribution and trafficking in vivo. *Curr. Biol.* **24**, 2059-2065. doi:10.1016/j.cub.2014.07.051

**Pielage, J., Fetter, R. D. and Davis, G. W.** (2006). A postsynaptic Spectrin scaffold defines active zone size, spacing, and efficacy at the *Drosophila* neuromuscular junction. *J. Cell Biol.* **175**, 491-503. doi:10.1083/jcb.200607036

**Price, T. J., Flores, C. M., Cervero, F. and Hargreaves, K. M.** (2006). The RNA binding and transport proteins staufen and Fragile X mental retardation protein are expressed by rat primary afferent neurons and localize to peripheral and central axons. *Neuroscience* **141**, 2107-2116. doi:10.1016/j.neuroscience.2006.05.047

**Ramirez, D. M. O., Khvotchev, M., Trauterman, B. and Kavalali, E. T.** (2012). Vti1a identifies a vesicle pool that preferentially recycles at rest and maintains spontaneous neurotransmission. *Neuron* **73**, 121-134. doi:10.1016/j.neuron.2011.10.034

**Ramos, A., Grünert, S., Adams, J., Micklem, D. R., Proctor, M. R., Freund, S., Bycroft, M., St Johnston, D. and Varani, G.** (2000). RNA recognition by a Staufen double-stranded RNA-binding domain. *EMBO J.* **19**, 997-1009. doi:10.1093/emboj/19.5.997

**Ramos, A., Hollingworth, D. and Pastore, A.** (2003). G-quartet-dependent recognition between the FMRP RGG box and RNA. *RNA* **9**, 1198-1207. doi:10.1261/rna.5960503

**Rana, M. S., Wang, X. and Banerjee, A.** (2018). An improved strategy for fluorescent tagging of membrane proteins for overexpression and purification in mammalian cells. *Biochem.* **57**, 6741-6751. doi:10.1021/acs.biochem.8b01070

**Renden, R. B. and Broadie, K.** (2003). Mutation and activation of Galpha s similarly alters pre- and postsynaptic mechanisms modulating neurotransmission. *J. Neurophysiol.* **89**, 2620-2638. doi:10.1152/jn.01072.2002

**Rohrbough, J., Rushton, E., Palanker, L., Woodruff, E., Matthies, H. J. G., Acharya, U., Acharya, J. K. and Broadie, K.** (2004). Ceramidase regulates synaptic vesicle exocytosis and trafficking. *J. Neurosci.* **24**, 7789-7803. doi:10.1523/JNEUROSCI.1146-04.2004

**Sandstrom, D. J.** (2011). Extracellular protons reduce quantal content and prolong synaptic currents at the *Drosophila* larval neuromuscular junction. *J. Neurogenet.* **25**, 104-114. doi:10.3109/01677063.2011.606577

**Sara, Y., Virmani, T., Deák, F., Liu, X. and Kavalali, E. T.** (2005). An isolated pool of vesicles recycles at rest and drives spontaneous neurotransmission. *Neuron* **45**, 563-573. doi:10.1016/j.neuron.2004.12.056

**Schmid, A., Hallermann, S., Kittel, R. J., Khorramshahi, O., Frölich, A. M. J., Quentin, C., Rasse, T. M., Mertel, S., Heckmann, M. and Sigrist, S. J.** (2008). Activity-dependent site-specific changes of glutamate receptor composition in vivo. *Nat. Neurosci.* **11**, 659-666. doi:10.1038/nn.2122

**Shah, S., Molinaro, G., Liu, B., Wang, R., Huber, K. M. and Richter, J. D.** (2020). FMRP control of ribosome translocation promotes chromatin modifications and alternative splicing of neuronal genes linked to autism. *Cell Rep.* **30**, 4459-4472.e6. doi:10.1016/j.celrep.2020.02.076

**St Johnston, D., Beuchle, D. and Nüsslein-Volhard, C.** (1991). Staufen, a gene required to localize maternal RNAs in the *Drosophila* egg. *Cell* **66**, 51-63. doi:10.1016/0092-8674(91)90138-O

**Sulkowski, M., Kim, Y.-J. and Serpe, M.** (2014). Postsynaptic glutamate receptors regulate local BMP signaling at the *Drosophila* neuromuscular junction. *Development* **141**, 436-447. doi:10.1242/dev.097758

**Sulkowski, M. J., Han, T. H., Ott, C., Wang, Q., Verheyen, E. M., Lippincott-Schwartz, J. and Serpe, M.** (2016). A novel, noncanonical BMP pathway modulates synapse maturation at the *Drosophila* neuromuscular junction. *PLoS Genet.* **12**, e1005810. doi:10.1371/journal.pgen.1005810

**Tenenbaum, C. M., Misra, M., Alizzi, R. A. and Gavis, E. R.** (2017). Enclosure of dendrites by epidermal cells restricts branching and permits coordinated development of spatially overlapping sensory neurons. *Cell Rep.* **20**, 3043-3056. doi:10.1016/j.celrep.2017.09.001

**Tokuda, S., Higashi, T. and Furuse, M.** (2014). ZO-1 knockout by TALEN-mediated gene targeting in MDCK Cells: involvement of ZO-1 in the regulation of cytoskeleton and cell shape. *PLoS One* **9**, e104994. doi:10.1371/journal.pone.0104994

**Tsang, B., Arsenault, J., Vernon, R. M., Lin, H., Sonenberg, N., Wang, L.-Y., Bah, A. and Forman-Kay, J. D.** (2019). Phosphoregulated FMRP phase separation models activity-dependent translation through bidirectional control of mRNA granule formation. *Proc. Natl Acad. Sci. USA* **116**, 4218-4227. doi:10.1073/pnas.1814385116

**Tsou, W.-L., Ouyang, M., Hosking, R. R., Sutton, J. R., Blount, J. R., Burr, A. A. and Todi, S. V.** (2015). The deubiquitinase ataxin-3 requires Rad23 and DnaJ-1 for its neuroprotective role in *Drosophila melanogaster*. *Neurobiol. Dis.* **82**, 12-21. doi:10.1016/j.nbd.2015.05.010

**Tsurudome, K., Tsang, K., Liao, E. H., Ball, R., Penney, J., Yang, J.-S., Elazzouzi, F., He, T., Chishti, A., Lnenicka, G. et al.** (2010). The *Drosophila* miR-310 cluster negatively regulates synaptic strength at the neuromuscular junction. *Neuron* **68**, 879-893. doi:10.1016/j.neuron.2010.11.016

**Upadhyay, A., Moss-Taylor, L., Kim, M. J., Ghosh, A. C. and O'Connor, M. B.** (2017). TGF-β family signaling in *Drosophila*. *Cold Spring Harb. Perspect. Biol.* **9**, a022152. doi:10.1101/cshperspect.a022152

**Verkerk, A. J., Pieretti, M., Sutcliffe, J. S., Fu, Y. H., Kuhl, D. P., Pizzuti, A., Reiner, O., Richards, S., Victoria, M. F., Zhang, F. et al.** (1991). Identification of a gene (FMR-1) containing a CGG repeat coincident with a breakpoint cluster region exhibiting length variation in Fragile X Syndrome. *Cell* **65**, 905-914. doi:10.1016/0092-8674(91)90397-H

**Wang, C.-H., Huang, Y.-C., Chen, P.-Y., Cheng, Y.-J., Kao, H.-H., Pi, H. and Chien, C.-T.** (2017). USP5/Leon deubiquitinase confines postsynaptic growth by maintaining ubiquitin homeostasis through Ubiquilin. *eLife* **6**, e26886. doi:10.7554/eLife.26886

**Ward, R. E., Lamb, R. S. and Fehon, R. G.** (1998). A conserved functional domain of *Drosophila* Coracle is required for localization at the septate junction and has membrane-organizing activity. *J. Cell Biol.* **140**, 1463-1473. doi:10.1083/jcb.140.6.1463

**Ward, R. E., Schweizer, L., Lamb, R. S. and Fehon, R. G.** (2001). The protein 4.1, ezrin, radixin, moesin (FERM) domain of *Drosophila* Coracle, a cytoplasmic component of the septate junction, provides functions essential for embryonic development and imaginal cell proliferation. *Genetics* **159**, 219-228. doi:10.1093/genetics/159.1.219

**Wegel, E., Göhler, A., Lagerholm, B. C., Wainman, A., Uphoff, S., Kaufmann, R. and Dobbie, I. M.** (2016). Imaging cellular structures in super-resolution with SIM, STED and Localisation Microscopy: A practical comparison. *Sci. Rep.* **6**, 27290. doi:10.1038/srep27290

**Yilmazer, Y. B., Koganezawa, M., Sato, K., Xu, J. and Yamamoto, D.** (2016). Serotonergic neuronal death and concomitant serotonin deficiency curb copulation ability of *Drosophila* platonic mutants. *Nat. Commun.* **7**, 13792. doi:10.1038/ncomms13792

**Yu, Z., Fan, D., Gui, B., Shi, L., Xuan, C., Shan, L., Wang, Q., Shang, Y. and Wang, Y.** (2012). Neurodegeneration-associated TDP-43 interacts with fragile X mental retardation protein (FMRP)/Staufen (STAU1) and regulates SIRT1 expression in neuronal cells. *J. Biol. Chem.* **287**, 22560-22572. doi:10.1074/jbc.M112.357582

**Zhang, Y. Q., Bailey, A. M., Matthies, H. J. G., Renden, R. B., Smith, M. A., Speese, S. D., Rubin, G. M. and Broadie, K.** (2001). *Drosophila* Fragile X-Related gene regulates the MAP1B homolog Futsch to control synaptic structure and function. *Cell* **107**, 591-603. doi:10.1016/S0092-8674(01)00589-X

**Zhang, M., Chen, D., Xia, J., Han, W., Cui, X., Neuenkirchen, N., Hermes, G., Sestan, N. and Lin, H.** (2017). Post-transcriptional regulation of mouse neurogenesis by Pumilio proteins. *Genes Dev.* **31**, 1354-1369. doi:10.1101/gad.298752.117

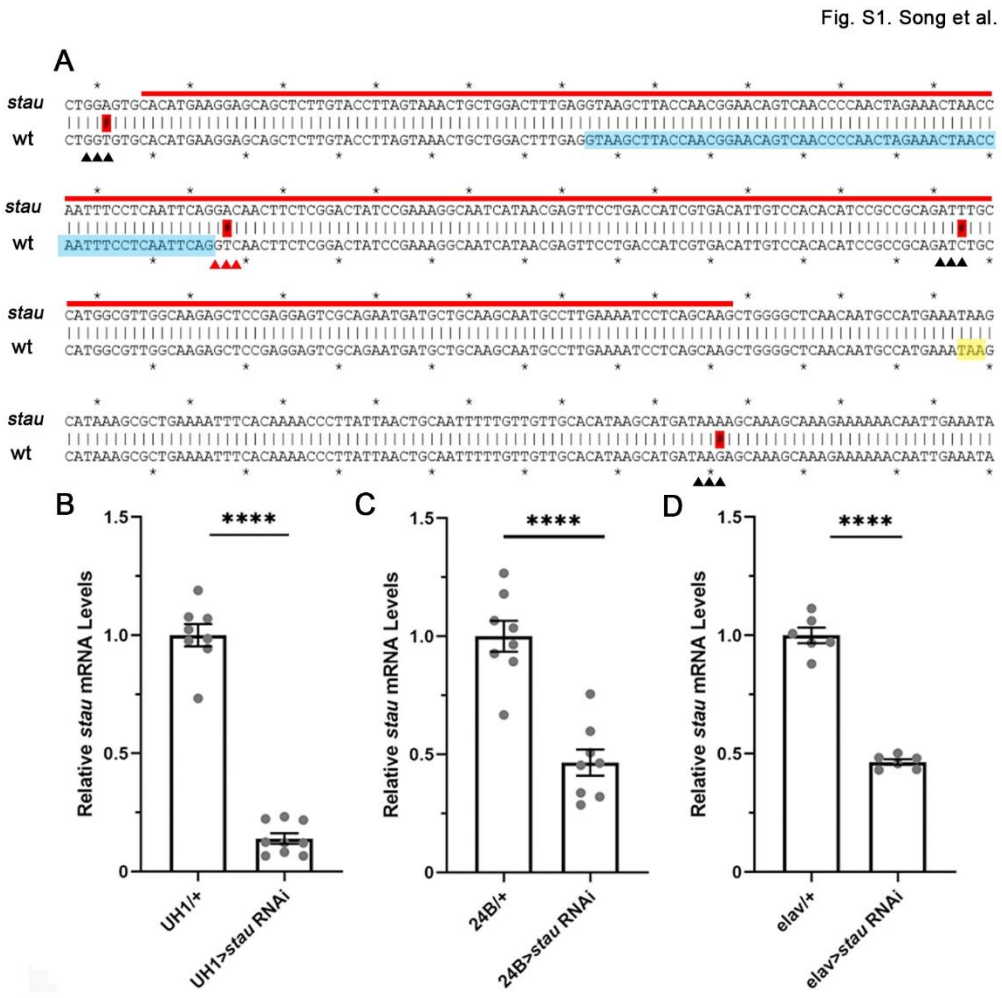


**Fig. S1. Mutant *staufen*$^{HL}$ sequence and *staufen* RNAi knock-down efficiency**

**(A)** The *staufen*$^{HL}$ mutant sequence compared to wildtype sequence (http://flybase.org/). The double strand RNA-binding domain 5 (dsRBD5, red underline) contains a single intron (blue shading). In the mutant, silent mutant codon (black triangles) and nonsense mutant codon (red triangles) with mutated nucleotide (red shading) upstream of the stop codon (yellow shading). **(B-D)** Larval qPCR measurements of *staufen* RNAi efficiency with ubiquitous UH1-Gal4 **(B)**, muscle-targeted 24B-Gal4 **(C)** and neuron-targeted *elav*-Gal4 **(D)**. Significance is indicated at p<0.0001 (****) based on student's *t*-tests.

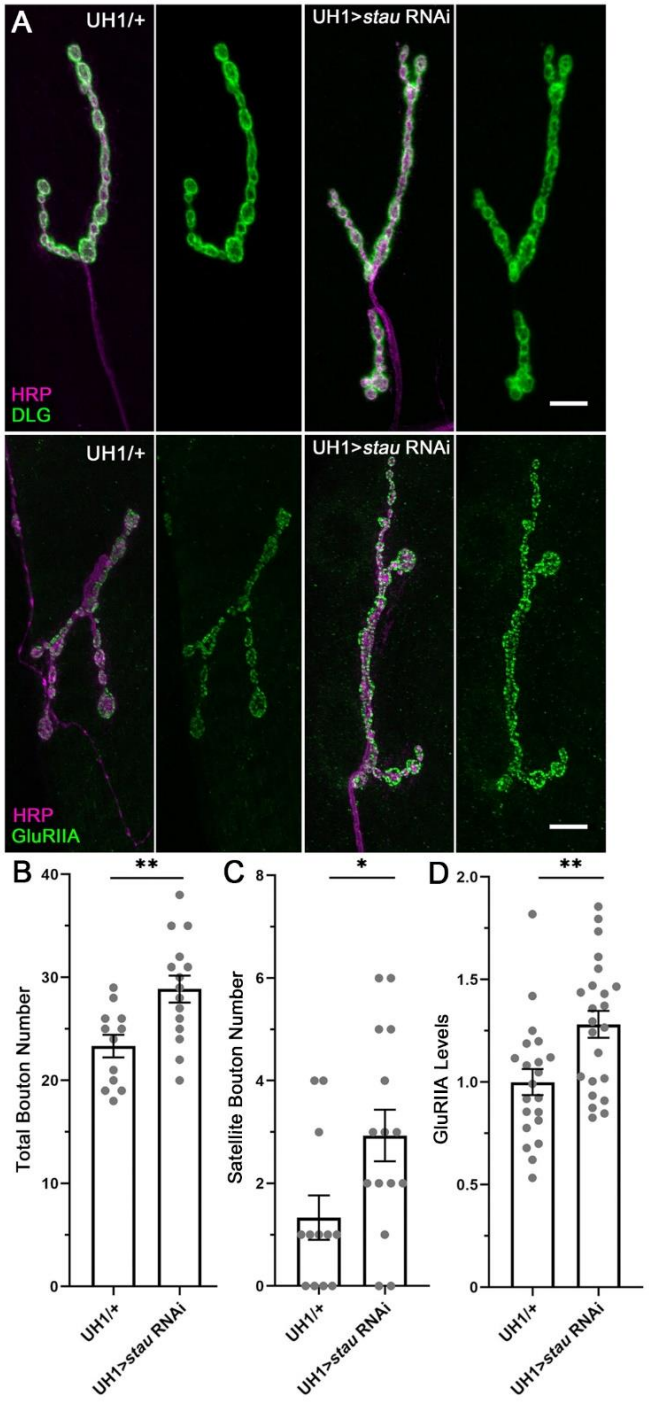


**Fig. S2. *staufen* RNAi increases synaptic bouton formation and GluRIIA levels**
Larval NMJ structure and GluRIIA levels compared between transgenic control (UH1/+) and staufen knockdown (UH1-stau RNAi). **(A)** Double labeling for presynaptic anti-HRP (magenta) and either postsynaptic DLG (green, top) or GluRIIA (green, bottom). Scale bar: 10 μm. Quantification of total synaptic bouton **(B)** and satellite bouton **(C)** number. **(D)** Quantification of GluRIIA fluorescence intensity normalized to genetic background control. Significance is indicated at $p<0.05$ (*) and $p<0.01$ (**) based on student's t-tests.

Fig. S3. Song et al.

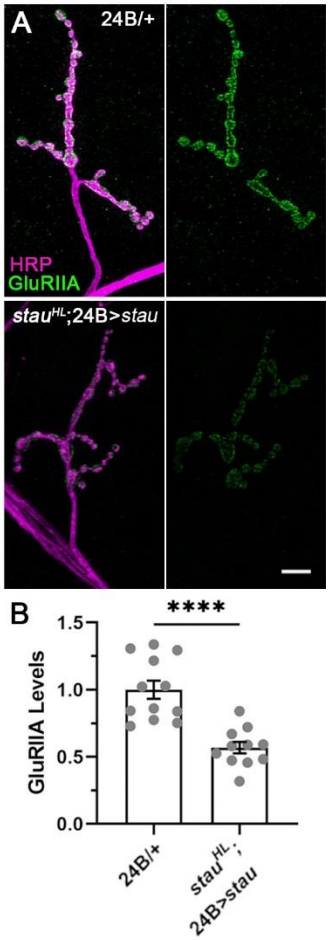


**Fig. S3. Postsynaptic muscle-targeted *staufen* rescue decreases GluRIIA levels**
Larval NMJs labeled for GluRIIA comparing transgenic control (24B/+) with postsynaptic muscle UAS-*staufen* expression in *staufen*$^{HL}$ (*stau*$^{HL}$) homozygous mutant background (*stau*$^{HL}$; 24B>*stau*). (**A)** Double labeling for both presynaptic anti-HRP (magenta) and anti-GluRIIA (green) in the 24B-Gal4/+ control (top) and muscle *staufen* rescue in the *stau*$^{HL}$ mutant (bottom). GluRIIA labeling alone is shown on the right for both genotypes. Scale bar: 10 μm. **(B)** Quantification of the normalized GluRIIA fluorescence intensity. Significance is indicated at $p<0.0001$ (****).

Fig. S4. Song et al.

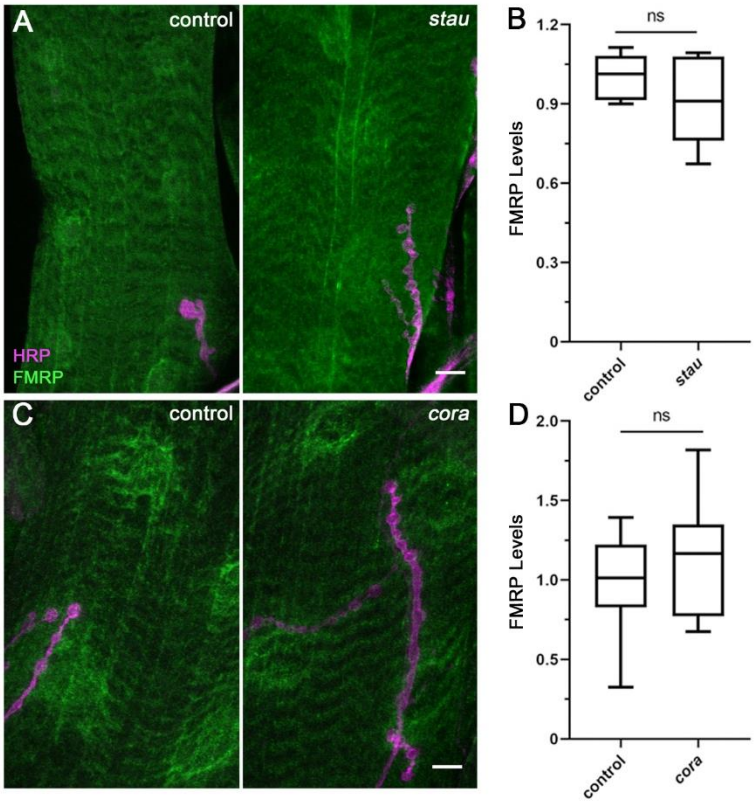


**Fig. S4. Neither *staufen* and *coracle* mutants affect muscle FMRP levels**

Larval muscles labeled for FMRP comparing genetic background control ($w^{1118}$) with *staufen* ($stau^{HL}$) and *coracle* ($cora^{14}$) mutants. **(A)** Double labeling for anti-FMRP (green) and synaptic anti-HRP (magenta) in control versus *staufen* mutant. Scale bar: 10 μm. **(B)** Quantification of FMRP levels shows no significant (ns) change. **(C)** Double labeling for FMRP (green) + HRP (magenta) in control versus *coracle* mutant. Scale bar: 10 μm. **(D)** Quantification of FMRP levels shows no significant (ns) change.

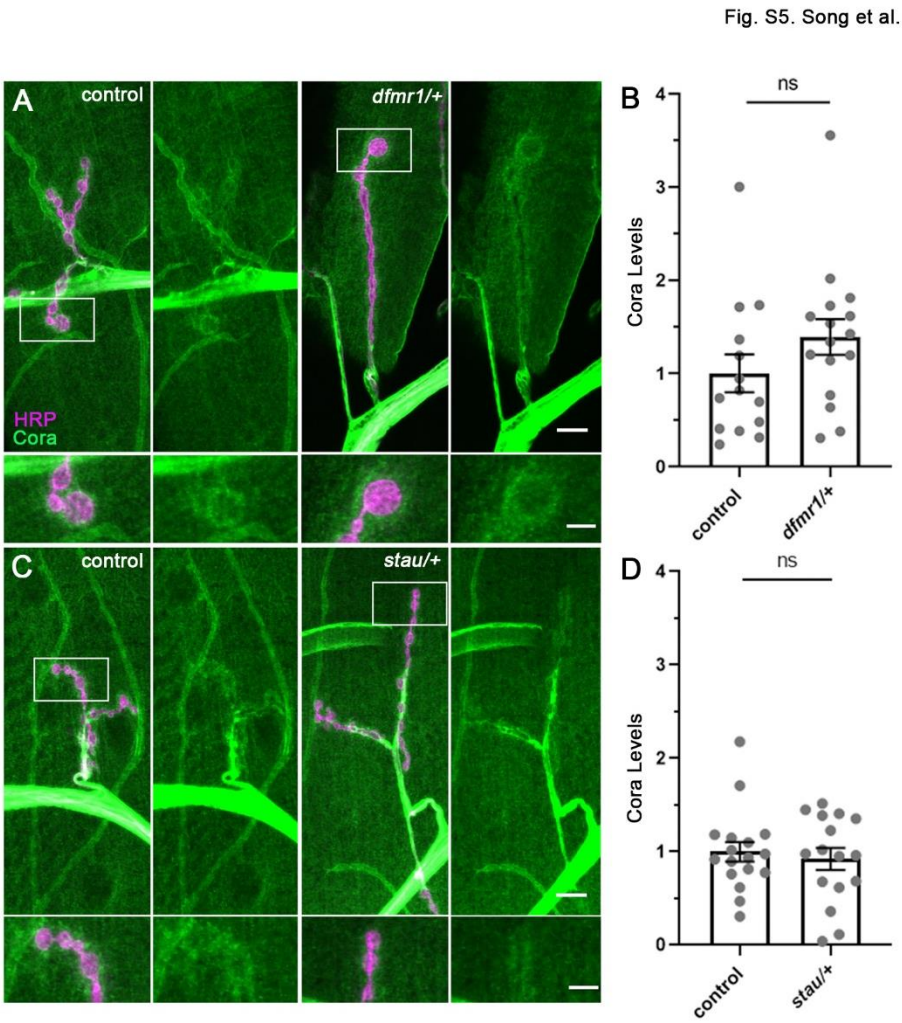


**Fig. S5. Heterozygous *dfmr1*/+ and *staufen*/+ do not affect Coracle levels**

Larval NMJs labeled for Coracle in controls ($w^{1118}$) compared to *dfmr1* ($dfmr1^{50M}$/+) and *staufen* ($stau^{HL}$/+) heterozygotes. Top rows show full muscle 4 NMJs (scale bar: 10 μm) with white-boxed regions shown magnified below (scale bar: 5 μm). **(A)** Double labeling for presynaptic HRP (magenta) and Coracle (Cora, green) in control versus *dfmr1* heterozygote. **(B)** Postsynaptic Coracle levels normalized to control show no significant (ns) change. **(C)** NMJ Coracle labeling shown in control versus *staufen* heterozygote. **(D)** Postsynaptic Coracle levels normalized to control show no significant (ns) change.

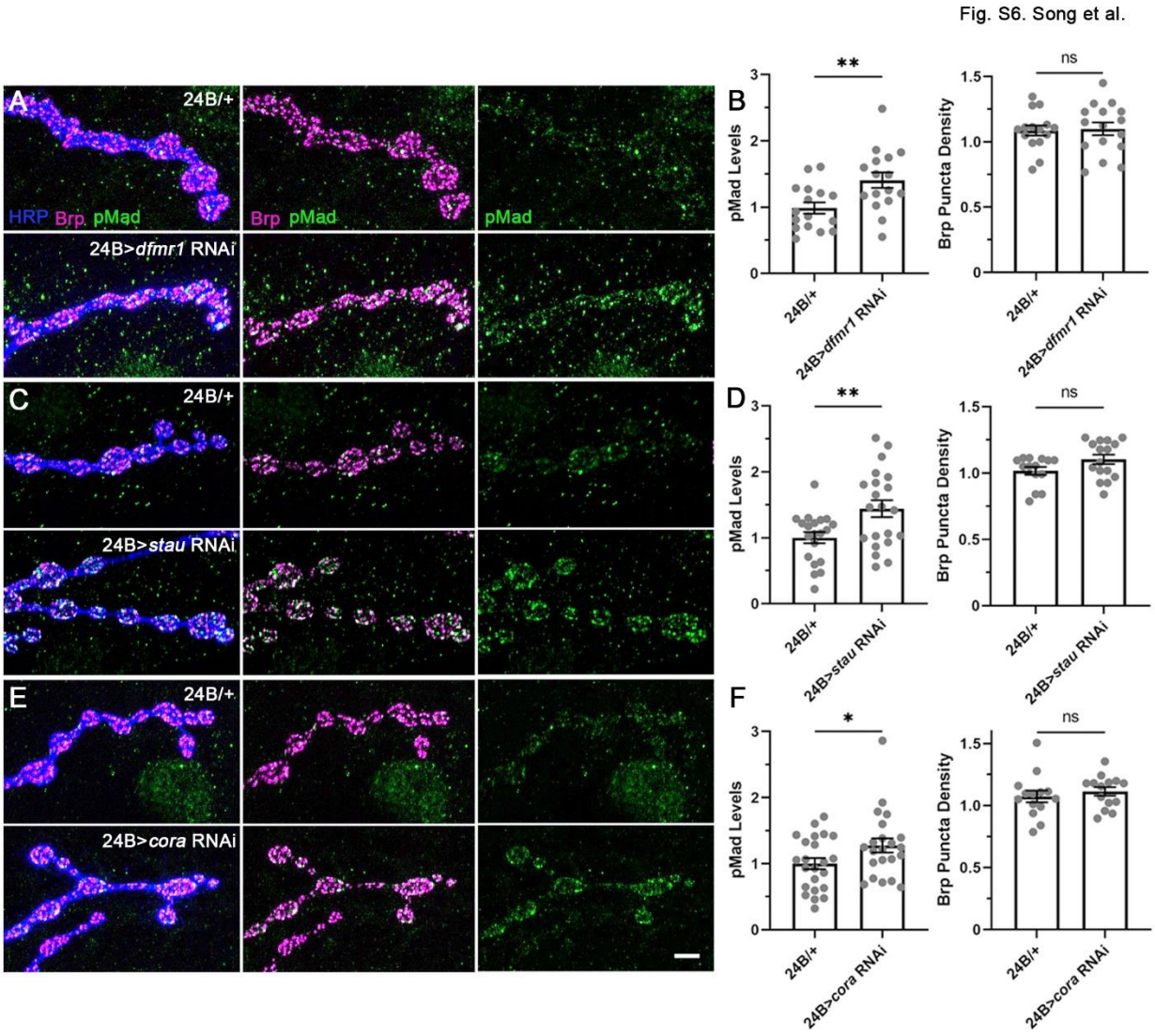


**Fig. S6. Postsynaptic FMRP, Staufen and Coracle all restrict pMad signaling**

Larval NMJs triple-labeled for HRP (blue), Brp (magenta) and pMad (green) in muscle driver controls (24B/+, top rows) and with *dfmr1* (24B>*dfmr1* RNAi), *staufen* (24B>*stau* RNAi) and *coracle* (24B>*cora* RNAi) knockdown. **(A)** Representative images of *dfmr1* postsynaptic RNAi. **(B)** Quantification of normalized pMad fluorescent intensity (left) and Brp active zone density (right). **(C)** Representative images of muscle-targeted *staufen* knockdown. **(D)** Quantification of pMad levels and Brp active zone density. **(E)** Images of *coracle* postsynaptic RNAi. Scale bar: 5 μm. **(F)** Quantification of presynaptic pMad levels and Brp active zone density. Significance is indicated at $p<0.05$ (*), $p<0.01$ (**) and $p>0.05$ (not significant; ns) based on student's *t*-tests.

**Table S1.** Transgenic UAS lines used in this study.

| Line | Provider | Reference |
|---|---|---|
| UAS-*stau* RNAi | VDRC 106645 | (Landskron et al. 2018) |
| UAS-*stau* RNAi | BDSC 31247 | (Mahoney et al., 2016) |
| UAS-*cora* RNAi | BDSC 51845 | (Jiang et al., 2019) |
| UAS-*dfmr1* RNAi | BDSC 35200 | (Flockhart et al., 2006) |
| UAS-myc-*cora* | Fehon Lab | (Ward IV et al., 1998) |
| UAS-*stau*-GFP | Ramaswami Lab | (Barbee et al., 2006) |
| UAS-YFP-*dfmr1* | Zarnescu Lab | (Cziko et al., 2009) |

**Table S2.** Primers used in this study.

| Primer (forward) | Sequence | Primer (reverse) | Sequence |
|---|---|---|---|
| Staufen | GTAAACTGCTGGACTTTGAGGTC | Staufen | GCAGCATCATTCTGCGACTCC |
| GAPDH | CGTTCATGCCACCACCGCTA | GAPDH | CACGTCCATCACGCCACAA |
| Tubulin | ATTTACCCAGCACCACAAGTGT | Tubulin | GGCGATTGAGATTCATGTAGGTGG |
| Futsch | TTCCTGGATATTGCAGGACGG | Futsch | CTCGGGCAATGTGTGCCATA |
| Coracle | AAGAACAAGAAGGAGAAGGATGC | Coracle | CATTAACAGCCGCTCCTGCAG |
| Pal1 | ACGACTGGGGCAAGAACTTTTTT | Pal1 | CGTAGGATATGCCGGAGAAGG |